The Thesis Committee for Stevenson Hardy Bunn
Certifies that this is the approved version of the following thesis:

Toward an accurate reservoir model of heterolithic, tidally-influenced deposits: An ongoing case study in the Sego Sandstone member of the Mancos Shale through second-generation, outcrop-to-subsurface 3-D modeling

APPROVED BY
SUPERVISING COMMITTEE:

Supervisor: _____
William L. Fisher

Co-Supervisor: _____
Lesli J. Wood

_____
Dallas B. Dunlap

Toward an accurate reservoir model of heterolithic, tidally-influenced deposits: An ongoing case study in the Sego Sandstone member of the Mancos Shale through second-generation, outcrop-to-subsurface 3-D modeling

by

Stevenson Hardy Bunn, B.A.

Thesis

Presented to the Faculty of the Graduate School of

The University of Texas at Austin

in Partial Fulfillment

of the Requirements

for the Degree of

Master of Science in Energy and Earth Resources

The University of Texas at Austin

May 2015

Dedication

I would like to dedicate this work to my family, whose unwavering love and constant support made this all possible.

Acknowledgements

I would like to acknowledge Dr. Bill Fisher and Dr. Lesli Wood for their continued support and guidance through my entire Masters process. I also appreciate all of the advice from Mr. Dallas Dunlap, Dr. Darrin Burton and Mr. Chris Dorion at Schlumberger.

This Masters project was made possible by the financial support of the Quantitative Clastics Laboratory Industrial Associates consortium including Anadarko, BHP Billiton, Cairn India, ExxonMobil, Marathon, Repsol, Maersk, Ophir, Inpex, Noble Energy, Statoil, and Woodside. Additional support for research opportunities was provided by the Energy and Earth Resources Program in the Jackson School of Geosciences.

Abstract

Toward an accurate reservoir model of heterolithic, tidally-influenced deposits: An ongoing case study in the Sego Sandstone member of the Mancos Shale through second-generation, outcrop-to-subsurface 3-D modeling

Stevenson Hardy Bunn, M.S. E.E.R

The University of Texas at Austin, 2015

Supervisors: William L. Fisher and Lesli J. Wood

Heterolithic tidal reservoirs are common in hydrocarbon settings around the world, but can be underestimated as a contributor to total resource volume due to their complex lithologic and architectural nature. A preliminary, static geologic model was built for the Sego Sandstone, a tidally influenced unit that outcrops in the Book Cliffs of eastern Utah, to investigate variables influencing model construction and subsequent fluid flow. The initial model, built with DecisionSpace software, utilized 39 outcrop logs and 36 adjacent subsurface logs. Six bounding surfaces provided the 3-D framework for a spatial and temporal grid containing six facies, each with unique lithology, permeability and porosity. In addition, bed thickness, bioturbation intensity, gamma response, and net sand percentage were noted in sections and utilized as modifiers in the model. Based on limitations of the previous DecisionSpace model results, a second-generation model was undertaken using Petrel software to investigate: 1. the differences between model design and construction within these two software packages, 2. petrel's ability to incorporate fine-scale

heterogeneities and smaller elements such as tidal channels, swatchways and zones of intense bioturbation, and 3. the impact of bar type morphology (confined versus unconfined) and associated shale distributions on fluid flow. Resulting models were used to investigate standard modeling techniques versus multiple-point geostatistical simulation and the construction of training images. Uncertainty analyses are performed on data parameters using successive property realizations to examine fluid flow connectivity between tidal bar-intrabar architectural elements. Model results show simulated architectural elements that match observed outcrop parameters, honor stacking patterns, and provide enhanced facies distribution predictions. Finally, software gridding algorithms are compared to identify which of these algorithms more accurately characterize subsurface geometries, and ensure best prediction of lithofacies distributions. Outcomes illustrate the importance of integrating subseismic scale data into reservoir models and will inform future work in characterizing tidally-influenced reservoir stratigraphy and modeling approaches utilizing outcrop and subsurface data.

Table of Contents

List of Tables

List of Figures

Chapter 1: Introduction and Geologic Setting

INTRODUCTION

Heterolithic strata deposited under the influence of tidal processes form reservoirs throughout some of the world's most prolific hydrocarbon basins. The potential for these units to contribute to the overall hydrocarbon volume is often overlooked or underestimated, due to their complicated lithologic and architectural nature. The depositional complexities of tidal environments contribute to the heterogeneous character of these deposits as a result of the temporal and spatial nature of tidal processes (Burton, 2011). This heterogeneity makes it essential to properly capture and model the internal structure, character, and morphologies of the architectural elements (AE's) that comprise tidally-influenced reservoirs (Pickering et al., 1988) as the original depositional framework is one of the most influential variables on fluid flow in hydrocarbon reservoirs (Tyler and Finley, 1991; White and Barton, 1997, 1999; Wood, 2004).

An assessment of the compositional and geometric variability of architectural elements through outcrop-to-subsurface analysis offers valuable data for reservoir characterization. The performance of any reservoir model is often primarily dependent on the quality of conditioning data inputs and geologic interpretation over the choice of modeling technique (Deveugle et al., 2013). Once these geologic factors are determined, an improved 3-D geologic model can be constructed to guide reservoir design and generate flow simulations for enhanced resource development.

Despite the productive nature of tidally-influenced shoreline and deltaic deposits as petroleum reservoirs, few ancient, well-documented examples can be found in literature (Wood, 2004). Decades of work on significant outcrop exposures of the Sego Sandstone and associated units provide a comprehensive and well-constrained geologic dataset for

detailed modeling. In addition, the Sego Sandstone sits within a larger, regionally well-documented depositional setting (Legler, 2014). Finally, extensive subsurface well penetrations of the exposed section are located immediately behind the outcrop and offer a keen opportunity for three-dimensional mapping of the Sego framework surfaces and placing of the outcrop petrophysical details into a larger seismic-scale framework.

The Sego Sandstone is best characterized for modeling through use of a hierarchical framework that includes, from smallest to largest, facies (petrophysically-distinct, genetically-related rock units), facies associations (stacks of genetically related facies, henceforth referred to as architectural elements), depositional systems tracts (formed of a spatial and temporal distribution of genetically related architectural elements; i.e. tidal bars, tidal channels, wave influenced shelf sands, etc.) and finally, sequences (composed of a variety of spatially and temporally distributed depositional systems; Wood, 2004; Burton, 2011). Each of the elements in this hierarchical framework provides a potential contributing parameter to variably affecting small and large-scale reservoir flow, but it is architectural elements, namely tidal bars, within the Sego Sandstone that are of critical economic importance in understanding reservoir framework as a key insight into the flow behavior of petroleum reservoirs (Wood, 2004; Burton, 2011). Within these tidal bar and bar complex architectural elements, specific attention must be paid to the expression of tidal channels, swatchway incisions, architectural differences between unconfined and confined tidal bars, and the influence of bioturbation layers in modifying basic sedimentology including porosity, permeability, and thus, connectivity of these elements. All of these are important if one is to capture the true nature of these elements as a reservoir. In addition, shale architecture varies within these bars depending on individual bar location (upcurrent or downcurrent relative to the shoreline), on bar depositional settings (within an estuary or on an open shelf) and on the nature and strength of the tidal signal influencing

the depositing systems (Burton and Wood, 2013). It is our intent to take into account all of these variables in the generation of a geologic model for a classic tidally-influenced shoreline reservoir system.

A first generation geologic model of the Sego Sandstone was built by researchers at the Bureau of Economic Geology in 2010, through data from an outcrop characterization and subsurface correlation (Wood, 2004; Burton et al., 2011; Dunlap et al., 2010). This early model provided an analysis on the fine-scale changes in facies distributions within a framework of key surfaces, systems tracts, and sequences. The model generation process goal, using Landmark Graphic Inc's DecisionSpace Earth Modeling software, was to investigate the transfer of geologic data from outcrop and the adjacent subsurface into the modeling environment. A secondary goal was then to analyze the influence of tidal bar distribution on flow connectivity in valley fill versus out of valley older, unconfined shelf bar deposits through a preliminary flow model. An example image from the DecisionSpace model is provided to demonstrate the model interface and provide a comparison for subsequent Petrel model results (Appendix A).

Despite achieving its primary goals, the DecisionSpace model did not fully characterize the depositional complexity that exists in outcrop and did not completely capture the flow dynamics between the Sego's architectural elements. The goal of this research is to produce a second-generation, Petrel-based model (Dunlap et al., 2012). We hypothesize that the Petrel-based software will improve the first model's limitations through advanced geostatistical modeling methods that better capture the nature of tidally-influenced elements through an improved representation of the geologic model.

The use of geostatistical methods in building realistic geological models has increased recently as a means to more comprehensively integrate known and interpreted data into reservoir characterization. Traditional methods such as the pixel-based sequential

indicator simulation (Journel 1983; Isaaks 1990; Srivastava 1992; Goovaerts 1997; Chiles and Delfiner 1999) and object-based (Boolean) method (Haldorsen and Lake 1984; Stoyan et al. 1987; Deutsch and Wang 1996; Holden et al. 1998) rely on the statistical significance of the variogram, which describes the degree of spatial dependence of a stochastic process (Matheron, 1963). These approaches suffer significant limitations in their capability to generate user-defined, geologically realistic model realizations (Caers 2004). Geostatistical modeling techniques, such as multiple-point statistics (MPS) (Journel, 1992; Guadriano and Srivastava, 1993; Strebelle, 2002) offer the capacity to address geologic complexity issues, while more successfully honoring input data. This approach will be further discussed in this chapter.

In summary, this research will explore an advanced geostatistical approach for modeling fine scale heterogeneities using a well-conditioned analog of a tidally-influenced reservoir system. By establishing an instructive Petrel methodology for constructing and populating a 3-D geocellular model, we can investigate the role of architectural elements (AE's) as critical reservoir framework geometries impacting fluid flow. Specific attention is given to modeling element geometries and lithotypes such as tidal channels, tidal bars, swatchways, and bioturbated layers, and other scales of heterogeneity that often go uncaptured in typical models. The capabilities of MPS as a preferred geostatistical method for accurately representing reservoir heterogeneity in geomodels will be discussed. Finally, the study also provides additional commentary comparing the results of the second-generation Petrel model with those of the first-generation DecisionSpace model.

PREVIOUS WORK AND GEOLOGIC SETTING: SEGO SANDSTONE

Significant work has been done characterizing the stratigraphy and depositional nature of the upper Campanian Sego Sandstone. The Sego member is largely exposed in

outcrop in the Book Cliffs of Utah and is comprised of tidally-influenced, progradational cycles of siliciclastic deposition originating from the Sevier orogenic belt and depositing into the Western Cretaceous seaway (Van Wagoner, 1991; Wood 2004). Exposure in this area is north-south strike-oriented and consists of a 60 to 80 meter thick, 50 to 60 km wide, and north-east to south-west oriented wedge of sandstone (Willis and Gabel, 2001). The member is interpreted as marine shelf sands and muds, inner-shelf tidal sandbars, valley fills, and estuarine sediments deposited within a tidally-influenced shoreline that experienced multiple regressions and transgressions (Wood, 2004).

The Sego is underlain by the Buck Tongue shale, deposited during a regional flooding event of the Mancos Shale, and is overlain by the Neslen Formation, characterized by aggradational, coastal-plain facies (Fisher 1936; Fisher et al. 1960; Franczyk 1989; Franczyk et al. 1990; Van Wagoner 1991; Hettinger and Kirschbaum 2002; Hettinger and Kirschbaum 2004; Burton, 2011). These units together comprise a portion of the Mesaverde Group, a thick interfingering of sand and shale wedges prograding eastward into the Mancos seaway (Fig 1.1; Hettinger and Kirshbaum, 2003; Burton, 2011). To the west, the Sego slowly transitions into the tidally-influenced fluvial middle mudstone member of the Castlegate Sandstone (Yoshida et al. 1996; McLaurin and Steel 2000; Hettinger and Kirschbaum 2003, Burton, 2011). The Sego is divided into Upper and Lower units by the transgressive Anchor Mine Tongue of the Mancos Shale and can be further subdivided into the lower Lower and upper Lower Sego units (Erdmann, 1934; Fisher et al., 1960), separated by the regionally extensive Lower Sego shale (Wood, 2004).

As a well-studied tidal depositional analog, several authors have proposed different sedimentologic and sequence stratigraphic interpretations and classifications of the Lower Sego Sandstone (Painter et al., 2013; Legler 2014). Initial interpretations by Van Wagoner (1991) focused on proximal tidal sandstones as tidal bar elements found exclusively in

shallow, vertically stacked incised valleys. In this scenario, the erosive basal sandstones overlie regional unconformities, or sequence boundaries. In contrast, this paper acknowledges the interpretation proposed initially by Willis and Gabel (2001) and later expanded upon by Willis and Gabel (2003), Wood (2004), Burton and Wood (2011) and Steel et al. (2012). This interpretation links tidal sandstones to tidal bars in confined and unconfined channel settings within a larger tide-dominated delta system that experienced regressive-transgressive shorelines. In this scenario, flooding surfaces cap regressive-transgressive transitions and delineate genetic sequence boundaries (Galloway, 1989). The regressive wedge is considered the highstand (HST) and falling-stage systems tracts (FSST) and the transgressive wedge is considered the transgressive systems tract (TST).

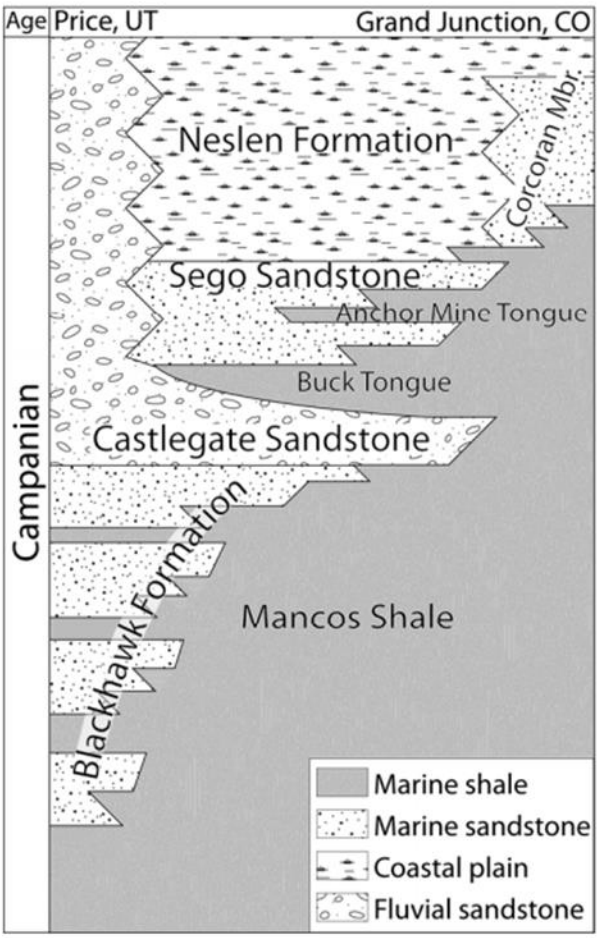

Figure 1.1: Lithostratigraphy of the Sego Sandstone and other formations that outcrop in the Book Cliffs of Eastern Utah (modified from Hettinger and Kirshbaum, 2003; Burton, 2011) from Grand Junction, Colorado (east) to Price, Utah (west).

TEMPORAL STRATIGRAPHY OF THE SEGO: CONCEPTUAL MODELS

Work by Wood (2004) documented the differences in tidal bar morphology within the various systems tracts of the Sego Sandstone. The initial highstand systems tract (HST) of Sequence 1 of the Sego is dominated by muddy, distal marine shelf facies. Within these units we see a higher percentage of continuous, thicker shales separating individual bar elements and stacked bar complexes. The HST experienced along-shore migration of

muddy sands with isolated, distal bars migrating into orientations perpendicular to the paleogeographic shoreline. Bedding surfaces in these deposits are likely to be parallel to shoreline, oriented by strike-directed shelf currents. As sea level fell, the deposits of this shelf were brought into the zone of storm and wave processes due to decreasing water depths and a regressive surface of marine erosion developed, overlain by the falling-stage systems tract (FSST) sediments. These deposits consist of progradational tidal bar complexes with decreased accommodation, resulting in increasing amalgamation, a higher number of bar forms and an increasingly sand-rich deposit. While shale beds in these FSST units are not as laterally continuous as in the deposits of the HST, they are prominent as abandonment drapes over bar stacks and individual bars. Bedding surfaces in the FSST deposits are more dip oriented as progradation dominates the falling shoreline. In contrast to the HST and FSST, the lowstand systems tract (LST) of the Sego is characterized by incised valley fills with migrating channels and bar forms. In reality, these are likely regions of estuarine environments. Increased sedimentation due to feeder system rejuvenation from a regressing shoreline contributes to a sand-rich system within valley-wall confined estuarine fairways, resulting in highly amalgamated, well-connected and highly permeable tidal bar complexes. However, such confined estuarine regions were not without their own stratigraphic complexity in the form of incisional swatchways, channel cuts and reworking of muddy tidal deposits into low permeability lags that often armor the base of channels or even the tops of bars. Bedding surfaces within the LST are more oblique to regional shorelines. Figure 1.2 depicts a complete diagram of the key stratigraphic framework of the Lower Sego.

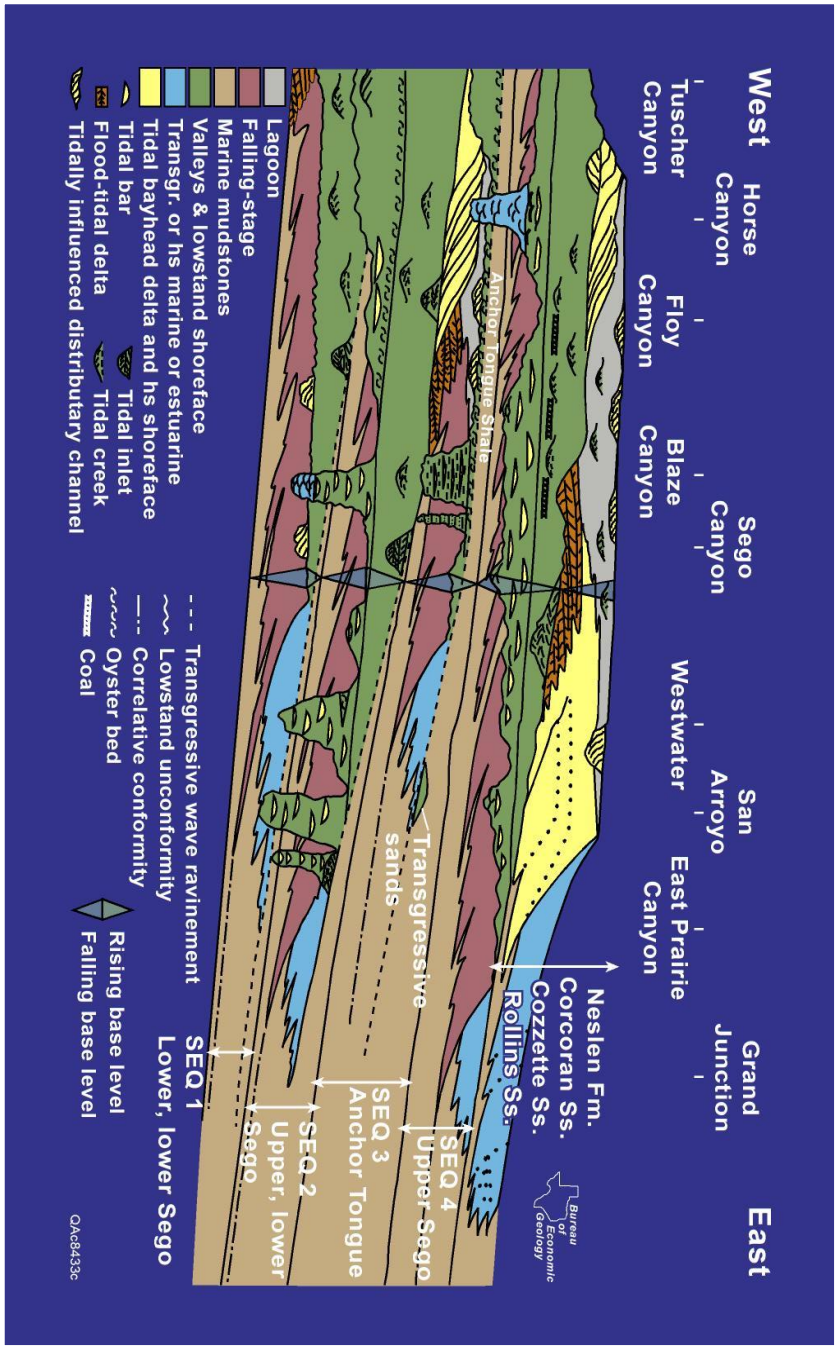

Figure 1.2: Sequence stratigraphic framework of the Sego Sandstone from Westwater Canyon, Utah to San Arroyo Canyon, Utah (after Wood, 2004). This diagram shows the three primary intervals being modeled in this study; Seq 1, Seq 2 and Seq 3.

Framing the model within the context of accommodation and sediment supply is important in understanding the size, distribution and spatial construction of AEs, which are all characteristics that potentially influence reservoir quality. Each of these variables will impact dynamic flow, specifically connectivity between reservoir elements. Figure 1.3a shows the FSST of Sego sequence 1 as a high accommodation falling limb deposit, characterized by a discontinuous, low relief RSME, and thicker falling-stage system deposit with little incisional valley development (Wood and Willis, 1999). Tidal bars within this scenario are more elongate and isolated. As sea-level rises, the Sego sequence 2 HST is deposited, still under high accommodation conditions, as a thick transgressive deposit with minimal ravinement on the marine flooding surface (Fig 1.3b). Tidal bars in the HST are more numerous and display a greater spatial distribution with the potential for increased amalgamation. Figure 1.3c shows the next overlying unit, the Seq 2 FSST occurring under much lower accommodation conditions than the Sego sequence 1 FSST resulting in a high-relief RSME, low downlap indices (i.e. distances between downlap termination points) and the development of significant overlying lowstand incised valleys that cut into the older strata (Wood and Willis, 1999). The development of incised valleys concentrates tidal bars within valley/estuarine fill, increasing their amalgamation and individual spatial extents. Figure 1.3d represents the paleogeography of a low accommodation transgression similar to what we believe occurred during the Anchor Mine Tongue flooding event. The deep wave ravinement occurring on the flooding surface and thin to nonexistent transgressive deposits are indications of low accommodation during sea-level rise (Wood and Willis, 1999). The result is a flooding shale that rapidly covered regions 100's of km inland of the lowstand shoreline, terminating sedimentation fairly rapidly over the study area.

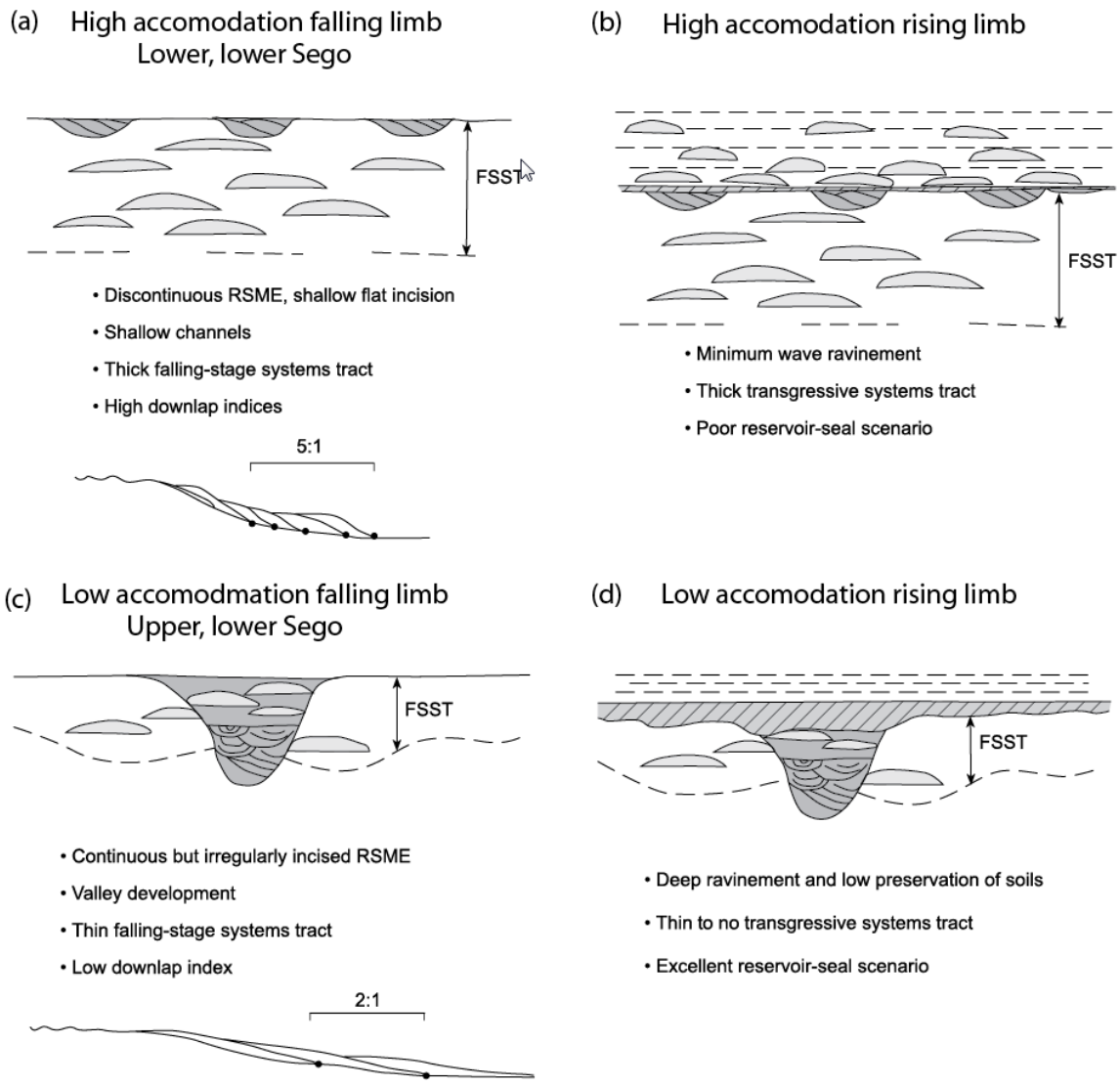

Figure 1.3: Diagram demonstrating the effects of high and low accomodation on sequence geometry in the Sego Sandstone (after Wood and Willis, 1999). Specific attention is given to the effects of acccomodation on the spatial variability and character of architectual elements, including tidal bars.

FACIES CLASSIFICATION OF THE SEGO SANDSTONE

Lithofacies are characterized as "a rock unit defined on the basis of its distinctive lithologic features, including composition, grain size, bedding characteristics, and sedimentary features" (Wood et al., 2004). The lower Sego units are composed of five primary facies, with distinct lithofacies. These include: 1. centimeter thick, wavy lenticular sandstones interbedded with shales (F1), 2. hummocky, cross-stratified sandstones (F2); 3. heterolithic, cross-stratified sandstone with abundant shale drapes (F3), 4. homogeneous, cross-stratified sandstone (F4), and 5. highly bioturbated sandstones (F5) (Fig 1.4; Wood and Willis, 1999; Willis and Gabel, 2001; Burton, 2011; Wood et al., 2004). These facies combine in various percentages and stacking patterns to build facies associations, referred to in this paper as architectural elements, which help define the sedimentary nature and depositional environments of the Lower Sego Sandstone.

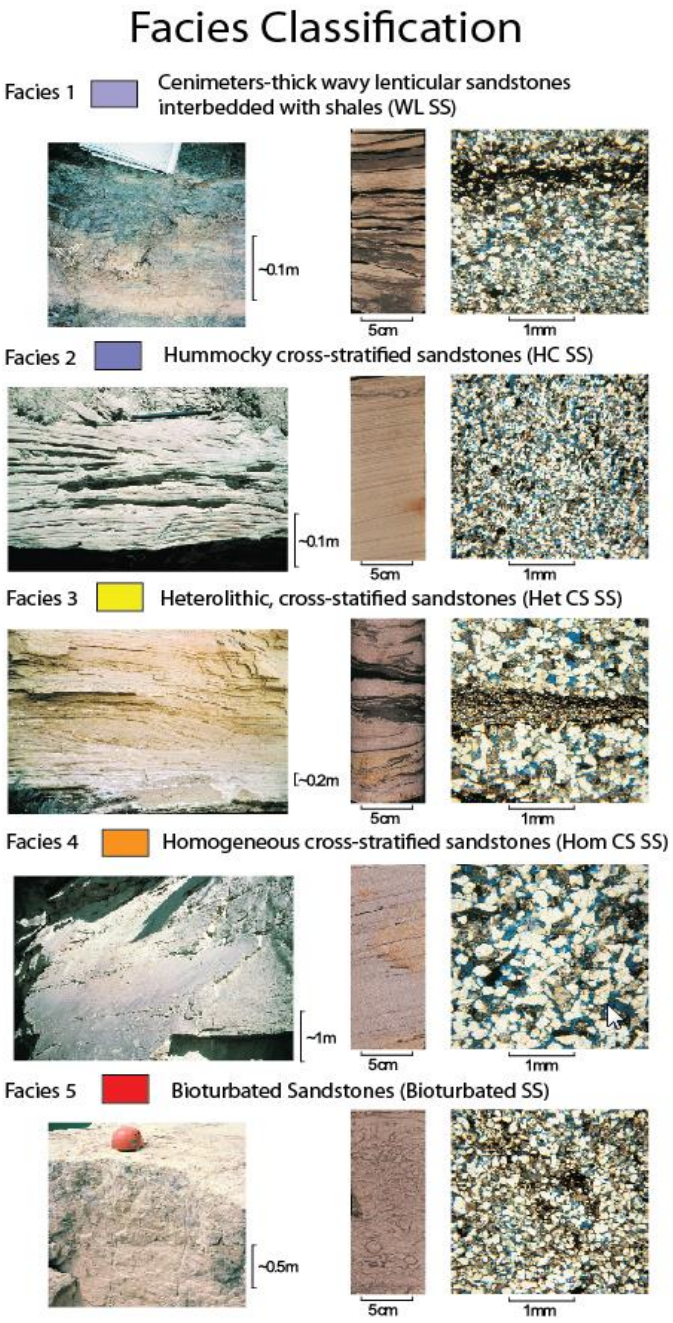

Figure 1.4: The five main petrophysically distinct facies of the Sego Sandstone. Associated colors and abbreviations were created for inputs in the second-generation Petrel model (after Wood and Willis, 1999; Willis and Gabel, 2001; Dunlap et al., 2012).

ARCHITECTURAL ELEMENTS OF THE SEGO SANDSTONE

Tidal bars, including both confined and unconfined, make up a high percentage of the architectural elements that compose the Sego Sandstone and are the Sego's key reservoir element (Wood, 2004). Tidal sandstones were principally deposited as migrating bars on a prograding delta front or proximal shelf (unconfined bars) or within the confines of estuaries, forming single row bank-attached bars (confined bars) (Burton, 2011). Deposition of unconfined tidal bars in the Sego is associated with a general falling-stage systems tract, while confined bars occur in incisional channels (over a kilometer wide) interpreted as a tidally-influenced, valley wall-confined estuary (Burton, 2011). Based on these different depositional environments, architectural and geometric heterogeneities exist. Tidal bars in the Sego average approximately 3.5 m in height, can be hundreds of meters wide and typically aggrade into larger tidal bar complexes (i.e. ridges) that can reach 11 m in height and with lengths greater than 4.5 km (Wood, 2004). Tidal ridges exhibit internal scour surfaces with basal incision by tidal-current processes as well as locally continuous internal shaly beds that may potentially serve as barriers or baffles to flow (Wood, 2004). In the Sego, individual tidal bars are primarily composed of Facies 3, 4, and 5.

The internal architecture of tidal bars can be complex due to superposition, where different bars deposit on one another forming amalgamated assemblages (tidal bar complexes of Wood, 2004) that make extraction of individual elements difficult (Dalrymple, 1995). This complexity is compounded by internal elements such as swatchways, which can occur in bi-directional confined settings. These swatchways may cross-cut bars and create variable incisional features that migrate along the length of elongate bars in response to dominant currents. These features often produce small-scale, lateral accretion deposits oriented at a high angle to the trend in the main bar (Dalrymple,

1995; Dalrymple and Choi, 2007). In localities such as San Arroyo Canyon, Utah, these swatchways can be seen cutting through more than 2.6 meters of tidal bar deposits and truncating underlying cross-sets (Wood and Flaig, 2012). Internally, these features are defined by heterolithic fill, including ripple laminated sandstones, zones of laminar sandstones and shales on the order of 10-20 cm. Thin layers of bioturbated sandstones and silts can also cap the more homogeneous sandstones as a result of slow sedimentation rates during swatchway abandonment. In general, confined bars are commonly shorter, thicker, narrower and more symmetric than unconfined bars, with the steeper side facing the direction of the locally dominant sediment transport direction. Table 1 provides a broad characterization summary and comparison between unconfined and confined bars in the Sego Sandstone (Burton, 2011).

	Unconfined tidal bars	Confined tidal bars
Depositional environment	Tidally-influenced delta front or tidal shelf	Estuarine valley fill
Facies succession (top) ↑ (base)	Bioturbated sandstone Homog. x-stratified sandstone Heterol. x-stratified sandstone	Homog. x-stratified sandstone Fluid muds/ clay clasts
Bar thickness	1.4-6.8 m	0.7-4.1 m
Organic material	Rare	Abundant (particularly in the base of valley fills)
Bioturbation	Common (especially bar tops)	Rare (dominantly isolated *Ophiomorpha*)
Gamma ray	Serrated to decreasing upward	Blocky increasing upward
Resistivity	Serrated to increasing upward	Blocky decreasing upward
Neutron porosity	Serrated to increasing upward	Blocky decreasing upward

Table 1.1: Characteristics of unconfined and confined tidal bar types in the Sego Sandstone (Burton, 2011).

STUDY AREA

The Petrel model study area covers a 12.8 km by 10.9 km region located in northeastern Utah, just north of I-72 and west of the Utah and Colorado border. The area encompasses a majority of the previously studied Eastern Outcrop Window (EOW) of the Book Cliffs (Fig 1.5; Van Wagoner, 1991). The outcrop dataset used to condition the second generation Petrel model consisted of 39 outcrop localities and included 10 centimeter interval core-scale descriptions of facies, bed thicknesses, bioturbation indices, gamma responses, permeability and porosity measures, and net sand percentages at each locality (Willis and Gabel, 2001; Wood, 2004). Detailed measured sections from outcrop and photopanel assisted correlations and the construction of a detailed 2-D stratigraphic framework. 2-D architectural element geometries and facies relationships were assessed

from this framework and interval bounding surfaces were correlated into the subsurface to the northwest of the outcrop using 36 outcrop adjacent well log suites. This correlation formed an initial framework for modeling. The original property modeling techniques from the first generation Decision Space model were re-created within Petrel to compare software results. This required using previously defined lithosets characterizing the hierarchical facies stacking patterns of tidal bar deposits and muddy sand deposits and assigning them to each stratigraphic interval (Dunlap et al., 2012).

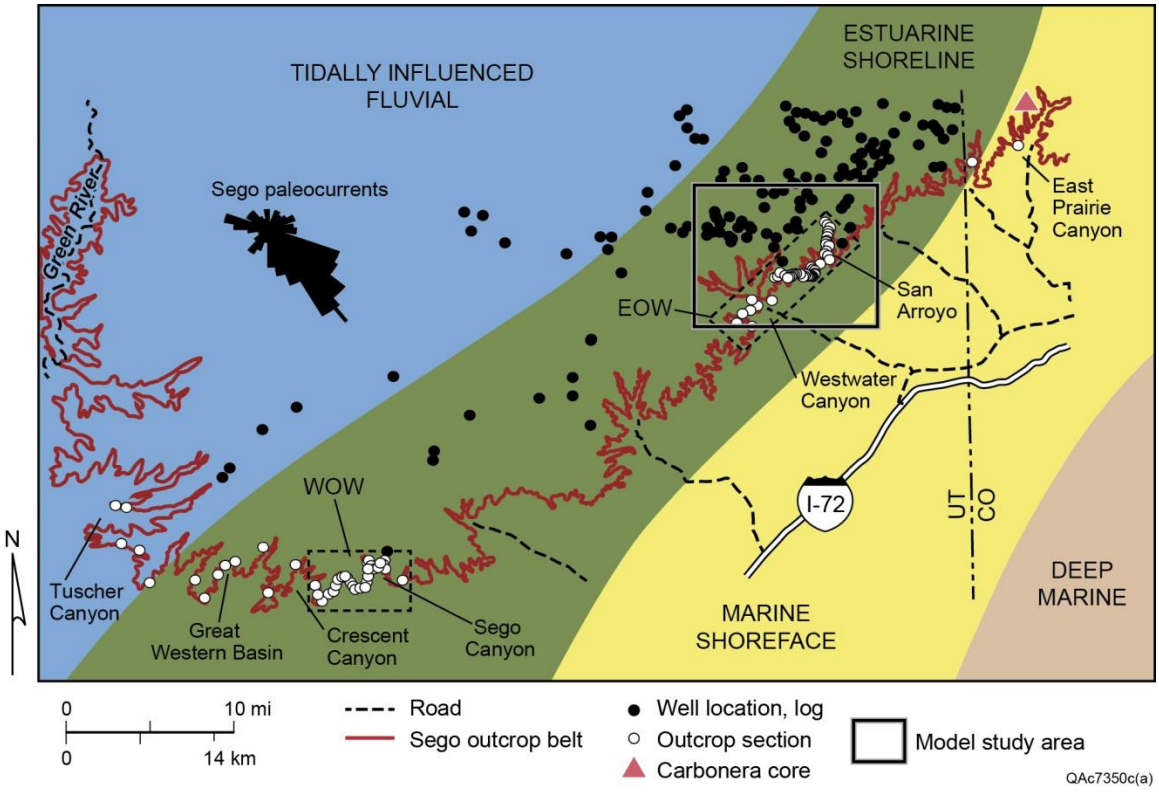

Figure 1.5: Map showing the exposed outcrop of the Sego Sandstone in the Book Cliffs of eastern Utah and western Colorado (red). The western outcrop window (WOW) and eastern outcrop window (EOW) designate previous, in-depth outcrop work by Van Wagoner (1991), Willis and Gabel (2001), Burton and Wood (2011) and others. Superimposed depositional tracts represent the paleogeography of the Sego Sequence 2 (upper, Lower Sego). Sego paleocurrents are after Willis and Gabel (2001). The area encompassed by the second-generation reservoir model is outlined in black and covers a 12.8 km by 10.9 km region.

METHODOLOGY

The methodology presented in this research is executed in three steps. Step one is the geologic characterization of the study area. Step two involves a multiple-point geostatistical modeling of data from the study area. Step three is the petrophysical modeling and preliminary flow analysis using the geostatistical model. Geostatistical modeling is performed using the Petrel-based MPFS (Multiple-point Facies Simulation)

algorithm, which should provide an opportunity to better integrate complex pattern recognition into training images and employ advanced property modeling capabilities to address the limitations of standard facies modeling techniques. The second-generation Petrel model also incorporates additional soft data properties that should better condition the model to reflect small-scale and large-scale heterogeneity within deposits of this tidally-influenced system. The introduction of soft data primarily includes the use of trend modeling and geometrical modeling to characterize the depositional complexity of the Sego.

Uncertainty and preliminary flow analyses are integrated through a series of probability (P10, P50, P90) and geometrical modeling to determine which model input parameters most affect simulation results and fluid flow behavior. An analysis of results from this study comments on the scale of heterogeneity within tidally-influenced reservoirs that is most impactful for generating accurate models and influencing recovery rates. Results will inform future work in characterizing tidally-influenced reservoir stratigraphy and modeling approaches integrating outcrop and subsurface data.

Chapter 2: Building the Geologic Model

Overview of Geostatistical Modeling Methods

Multiple statistical modeling tools and techniques exist for addressing reservoir characterization and constraining reservoir properties, based on the manipulation of geologic input data. The use of geostatistics is beneficial as it provides an automated approach to building multiple reservoir simulations capable of high process modeling and integrating multiple types of geologic and petrophysical data (Caers, 2004). These geologic models are then capable of generating direct realizations for use in flow simulations.

Traditional geostatistical methods for stochastic modeling, such as Sequential Indicator Simulation (SISIM) or Sequential Gaussian Simulation (SGSIM), are widely used cell-based modeling techniques that integrate a kriging-based algorithm, which relies on a variogram to establish spatial correlation between two points. Sequential simulations function by utilizing conditional distributions to mimic the covariance of attributes to provide simulated values from a random sequential path through adjacent data (Arpat, 2005). These methods, however, often fall short of capturing and honoring large, complex, and often continuous geologic features as low values tend to be overestimated and high values underestimated (Arpat 2005; Michael et al., 2009). A significant proportion of industry continues to utilize kriging-based geostatistical methods, but recent research is pushing past the limitations of traditional two point statistics and the variogram in favor of more advanced methods that greater characterize geologic and reservoir complexity.

Multiple-Point Statistics (MPS)

In constrast to kriging, Multiple-Point Statistics (MPS), first proposed by Journel (1992), measures the correlation between an unknown and multiple data points to characterize spatial distribution (Journel 1992; Caers 2004). MPS effectively combines

the strength of both pixel-based and object-based statistical techniques in its ability to spatially represent geologic complexity and reservoir heterogeneity (Strebelle, 2002; Caers and Zhang, 2002). MPS comprises simulations such as SNESIM (Single Normal Equation Simulation), FILTERSIM (Filter-based Simulation), or SIMPAT (SIMulation with PATterns) to condition data for enhanced simulations, however such conditioning can be difficult (Strebelle, 2002; Arpat and Caers, 2007; Michael et al., 2009; He et al., 2014). The latest version of Petrel uses the MPFS algorithm, which is a pixel-based method for creating facies models.

The MPS algorithm relies on the use of a Training Image (TI) to determine probability compared with the traditional variogram, which requires a fundamental understanding of the geologic representation and patterns trying to be modeled. Training images require the application of an idealized 3-D grid that represents spatial, variance, connectivity, heterogeneity, and spatial facies relationships and can generate multiple representations reflecting geologic uncertainty within a model (Pejman, 2012). Once created, training images successfully function as a database of user-defined patterns and geological property distributions for MPS. The MPS algorithm allows for the use of multiple training images for a multi-scale approach to defining reservoir variability and heterogeneity (Caers and Zhang, 2002).

Object-based geostatistical methods, or Boolean techniques, are commonly used as direct inputs for training images or are used indirectly to guide spatial distribution in constructing geologic patterns (Michael et al., 2009). This requires an initial image that is small enough for pattern duplication, but at least twice as large as the largest geological object trying to be reproduced. Training images should represent the approximate distribution of facies proportions in each region as well as contain a high degree of stationarity and ergodicity to generate successful representations of geological

relationships (Caers and Zhang, 2002). Training images provide substantial capabilities beyond variogram-based modeling techniques, primarily in their ability to better reproduce geological heterogeneities (Journel, 2005; He et al., 2014)

Limitations of the MPS technique include a potential nested modeling approach, which can create a complex hierarchical model that requires significant computational time. Through this approach, significant variance in facies distributions may not be fully preserved.

BUILDING THE GEOLOGICAL MODEL

3-D Grid Construction

To begin the modeling process, the initial project settings of the prior DecisionSpace model were re-created in Petrel including a NA-1927 datum and meter coordinate system. Using the vertical pillar gridding tool under structural modeling, a new Sego model was defined and a non-faulted 3-D grid was generated to develop the geo-cellular framework. Grid dimensions were bounded by a user-defined polygon converted to a grid boundary of the study area with 208 x 186 x 281 (I, J, K) grid cells. Individual grid cells were defined as 58.5 m (I) x 58.5 m (J) x 0.3 m (K). Following grid construction, previously correlated key stratigraphic surfaces were imported from the DecisionSpace model in stratigraphic order including the basal surface of the Buck Tongue (S-BT), first regressive surface of marine erosion (S-RSE1), the flooding surface (S-FS1), the second regressive surface of marine erosion (S-RSE2), and the Anchor Tongue (S-AT) (see sequence stratigraphy section for details). Surfaces were then each assigned "*conformability relationships*" to honor stratigraphic relationships and erosional characters. Figures 2.1 and 2.2 demonstrate how the model accurately represents the internal structure and conformability relationships of key bounding surfaces and

morphology within the Sego. After the surfaces were imported, intervals were generated through geometrical modeling to create reservoir intervals between the six stratigraphic control surfaces. Stratigraphic layering within intervals was also added as follows: Interval 1 = 86 (layers between S-BT and S-RSE1); Interval 2 = 49 (layers between S-RSE1 and S-FS1); Interval 3 = 22 (layers between S-FS1 and S-RSE2); Interval 4 = 64 (layers between S-RSE2 and S-LS1); Interval 5 = 86 (layers between S-LS1 and S-AT). Layers were used to maintain an average stratigraphic thickness of 0.3 meters between different intervals. The resulting grid contained 10,871,328 cells and 281 geological layers.

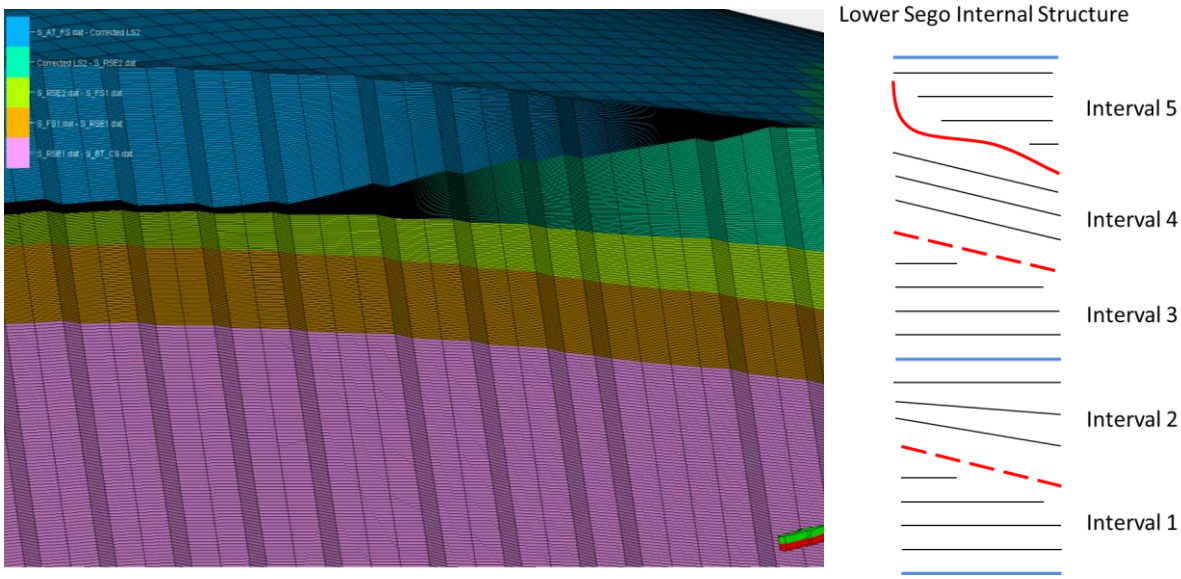

Figure 2.1: 3-D model honoring grid geometries and conformability relationships within the Lower Sego Sandstone. Vertical exaggeration is set to 15. The image was taken from Petrel using Gadwin PrintScreen.

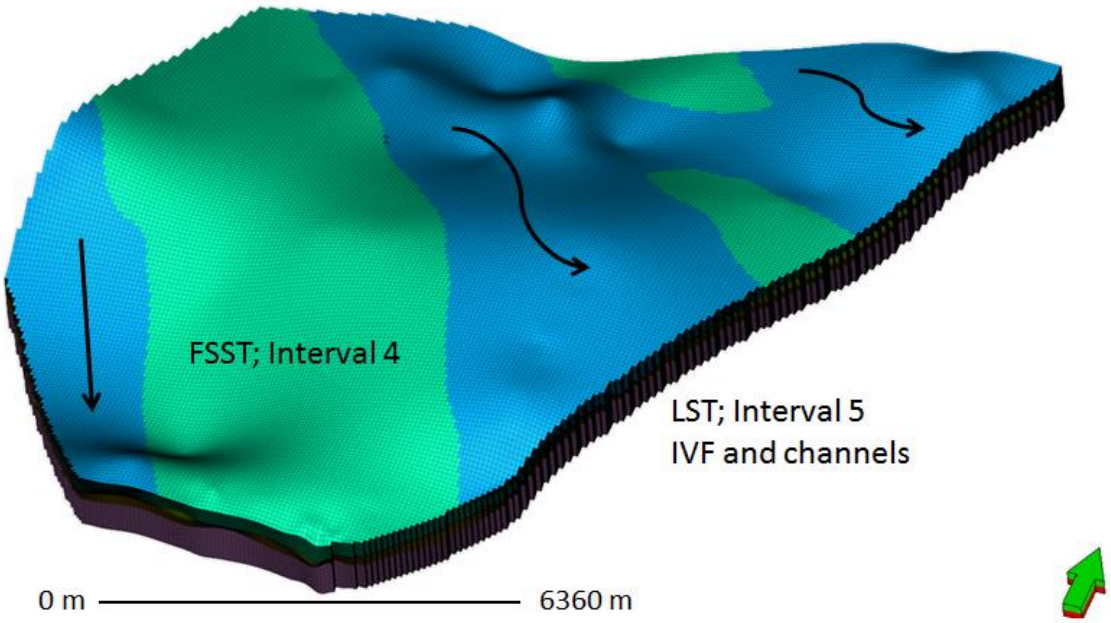

Figure 2.2: Grid of LST 2 interval illustrating deposition confined to the lowstand incised valley (blue) and lack of deposition over the interfluve areas where units of the underlying older Sego 2 FSST interval (green) are exposed. The grid area is 12.8 km by 10.9 km. Vertical exaggeration is set to 15. The image was taken from Petrel using Gadwin PrintScreen.

Grid construction was followed by a transfer of previously entered data from DecisionSpace to the new Petrel interface, which required significant data management and quality control. Importation of well lithofacies from Log ASCII Standard (LAS) files yielded a Petrel-assigned default facies template, thus a new facies and color template were created to match the first phase model and to ease comparison between the DecisionSpace model and the new Petrel model. Lithofaces were assigned from outcrop data and subsurface interpretations were honored and assigned as follows: 0 – outer/mid-Shelf mudstone (OS MS); 1 – wavy, lenticular sandstone (WL SS); 2 – hummocky, cross-stratified sandstone (HC SS); 3 – heterogeneous, cross-stratified sandstone (Het CS SS); 4 – homogeneous, cross-stratified sandstone (Hom CS SS); 5 – bioturbated sandstone

(Bioturbated SS)(Fig 1.4). Previous picks of the Lower Sego made in DecisionSpace were also extracted, formatted, and imported to ensure quality control in defining facies associations. Facies logs were then upscaled to the resolution of the 3-D grid using the Petrel-defined arithmetic average and neighborhood cell method.

Basic Property Modeling

Facies distributions within each interval were first modeled using a Truncated Gaussian geostatistical methodology after the DecisonSpace Plural-Gaussian method to compare software modeling results and provide a basis for further model conditioning. A seed number of 423,141 was used in each interval simulation to compare results with the DecisionSpace model and provide consistency of outcomes between realizations (If the model was not seeded manually, the outcome would be a different realization each time, making it difficult to investigate individual parameters on the modeling process). Vertical proportion curves were generated as inputs for vertical trends to constrain bias caused by a lack of well data density, to guide facies proportions for greater geologic characterization and to mimic the first-generation DecisionSpace method proportion function. Pre-defined tidal bar and muddy facies lithoset parameters were used to honor vertical stacking patterns, facies percentages within each interval, and guide variogram design (Table 2). A comparison between these basic geostatistical algorithm approaches is discussed later.

Systems Tract	Interval	Facies Associations	Primary axis (degrees)	Primary scale (ft)	Secondary scale (ft)	Vertical scale (ft)
LST	5	Muddy	160	4000	2000	6
		Bar Forms	160	6000	2000	40
FSST	2, 4	Muddy	135	8000	6000	8
		Tidal Bars	135	15000	5000	15
HST	1, 3	Muddy	45	24000	12000	10
		Distal Bars	135	10000	5000	14

Table 2.1: Input parameters by systems tracts for modeling facies association distributions within each Sego interval (seed number 423,141)(Burton, 2011).

Advanced Property Modeling in the Sego

Two training images (TIs) were generated (TI-1 and TI-2) and used to represent the spatial nature of AEs during two phases of shoreline position. The images could be combined in different spatial percentages to represent the paleogeographic character of the landscape during highstand, falling-stage, or lowstand of shorelines. The two training images were created with 100 x 100 x 20 (IJK) grid cells (with each grid cell equal to 58.5 m x 58.5 m x 0.3 m as defined in grid construction) and with an individual cell size (XYZ) set at 1 grid cell unit for property modeling using MPSF. Each TI was given an ellipsoid

search mask with 10 x 10 x 3 (IJK) grid cell units and an effective radius of 40 x 40 x 12 (IJK) grid cells to generate a pattern. An ellipsoidal search mask is preferred over a rectangular mask as it enhances the simulation run time of the MPS algorithm (Petrel Advanced Property Modeling Training and Exercise Guide, 2013). Three multi-grids, which are used to determine the coarseness of a grid, were also used with a subgrid of 32 grid cells to generate a more efficient simulation while maintaining large-scale continuity within the realization. Each interval, formed through TI application, differs with respect to architectural elements and facies distribution parameters based on the static paleogeomorphology of the Sego at a time of falling stage, lowstand, or highstand shoreline conditions, thereby depicting more medial, proximal, or distal environments, respectively (Fig 2.3-2.5). Regions were generated on each layer through user-defined polygons, assigned a one or two depending on the corresponding training image, and then merged using the property modeling calculator (Fig. 2.6) to capture the transition between depositional environments.

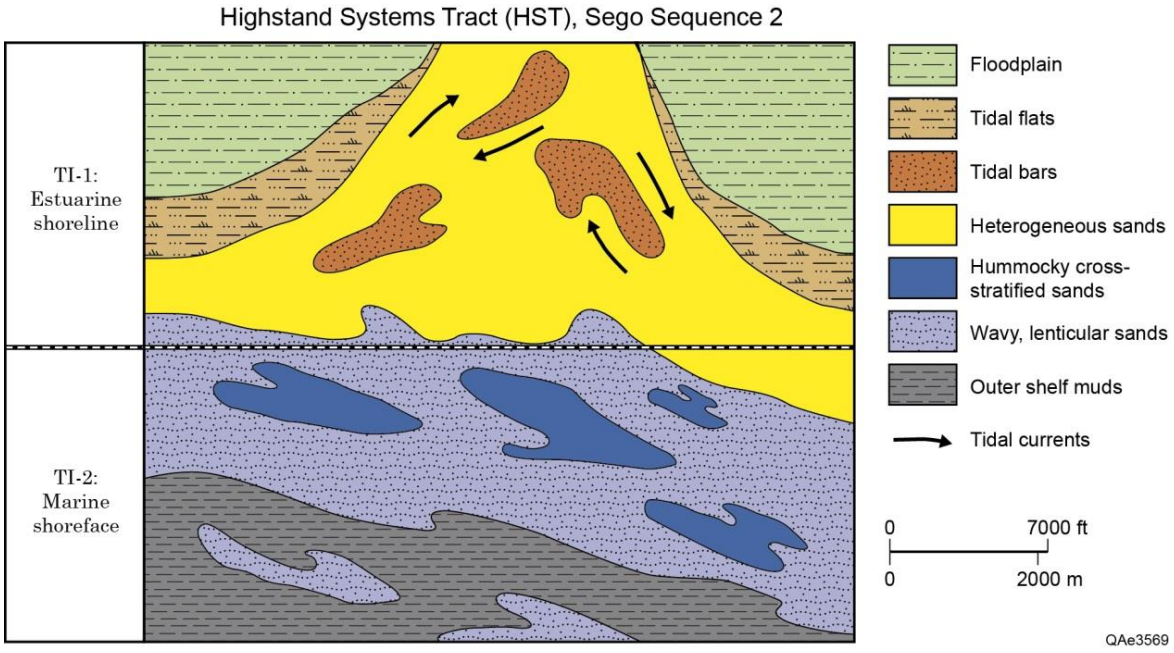

Figure 2.3: Expected facies distribution patterns during the HST of Sego Sequence 2. The dotted line serves to delineate TI regions and associated training image patterns based on depositional changes between the Sego esutarine and marine environments.

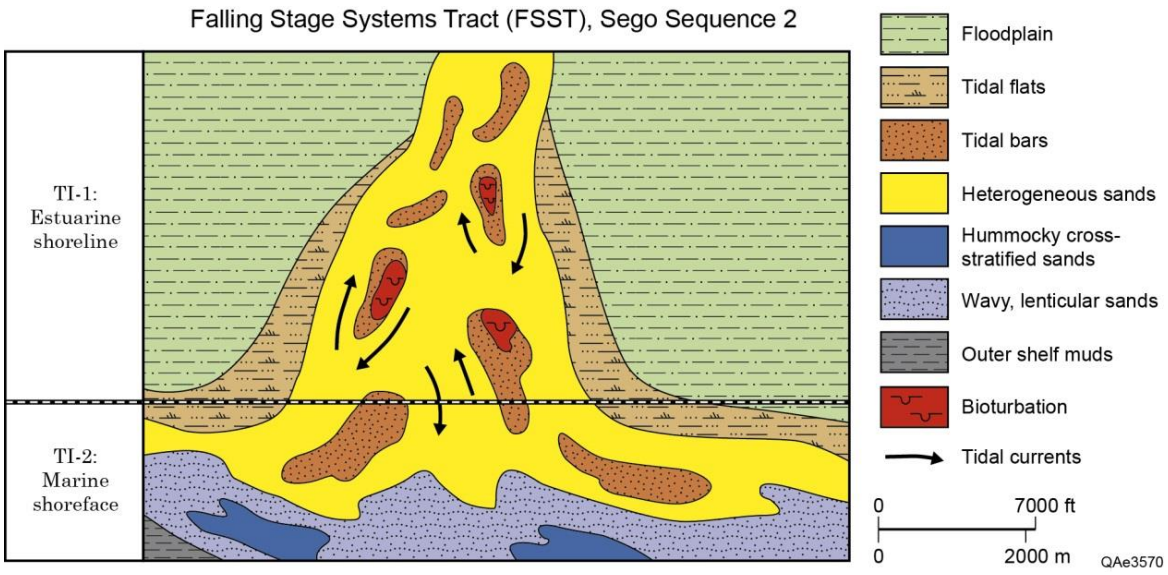

Figure 2.4: Expected facies distribution patterns during the FSST of Sego Sequence 2. The dotted line serves to delineate TI regions and associated training image patterns based on depositional changes between the Sego estuarine and marine environments.

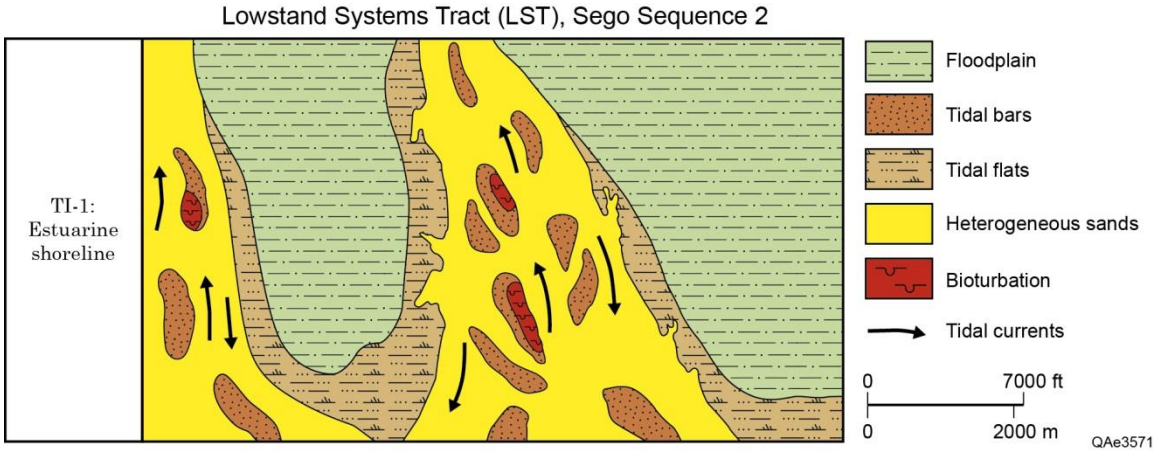

Figure 2.5: Expected facies distribution patterns during the LST of Sego sequence 2.

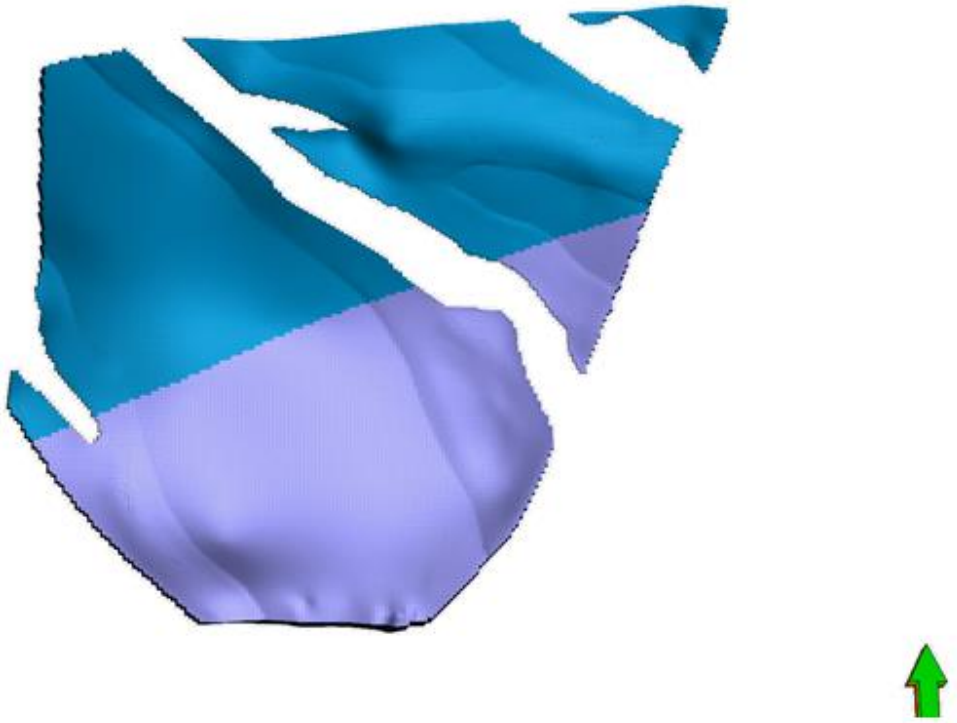

Figure 2.6: Grid of the Sego 2 FSST of interval 4 demonstrating the regions concept. Region 1 (teal) corresponds with the more proximal, estuarine shoreline of the Sego (60%) and transitions into region 2 (purple) representing the Sego marine shoreface environment (40%). Regions were produced with the equation New_Region = If (Region1_FSST_4 = 1. Region1_FSST_4, Region) where Region1_FSST_4 is = 1 and Region = 2. The grid covers a 12.8 km by 10.9 km study area Vertical exaggeration is set to 15. The image was taken from Petrel using Gadwin PrintScreen.

Training Images

Training image one (TI-1)(Fig. 2.7) represents a widening of valleys within the Sego and the creation of confined tidal bar complexes whose orientation radially flares as the valley meets the open marine shelf. Tidal bar facies associations are emplaced within a sandier channel matrix (F3) and become more elongate in the direction of the marine shelf as the incised valley widens distally. Tidal bar tops may also be bioturbated. TI-1 is most represented in the study area during the Sego FSST and LST.

TI-1 was constructed using the Truncated Gaussian method, with tidal bar associations set to a background property of heterogeneous cross-stratified sands (F3). Truncated Gaussian was used over simple object modeling of tidal bars to better preserve facies associations. Property statistics were selected based on facies proportions from upscaled logs. In the Petrel modeling software, under the variogram geometry tab, tidal bar dimensions and orientations were defined based on first-generation model parameters using an ellipse body shape, with rounded radial profile (Table 2). Tidal bar facies association input parameters from outcrop measurements for TI-1 were changed between realizations to reflect the specific modeled interval.

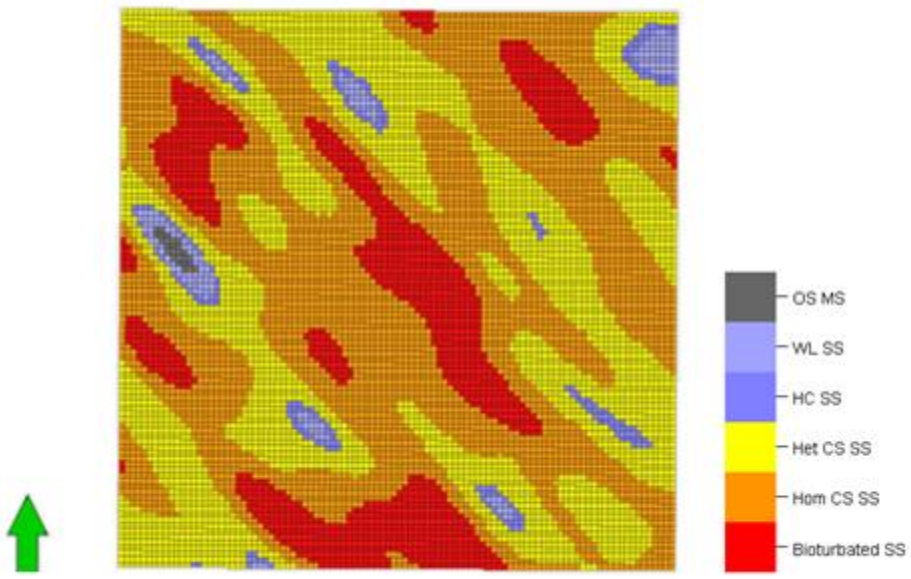

Figure 2.7: Adaptation of training image one representing the FSST of interval 4. The training image grid is a 30.4 m x 30.4. x 9.1 m. Tidal bars are comprised of homogeneous sands (F4) with bioturbated tops (F5) in a heterolithic sand matrix (F3) underlain by muddy bar facies (F1 and F2). The image was taken from Petrel using Gadwin PrintScreen.

An additional training image was generated to capture swatchway features through object modeling (Fig 2.8) and integrated into TI-1 for the Sego sequence 2 LST through a hierarchical modeling workflow hinged on the assign values method (Fig 2.9). This allowed for stochastic placement within previously modeled tidal bars. Swatchways were modeled as adaptive channels filled with heterogeneous sands (F3) and assigned continuous, stochastic shales (F0). Swatchways were also given a range of orientations from 130-190 degrees. Parameters were estimated off of observed outcrop measurements.

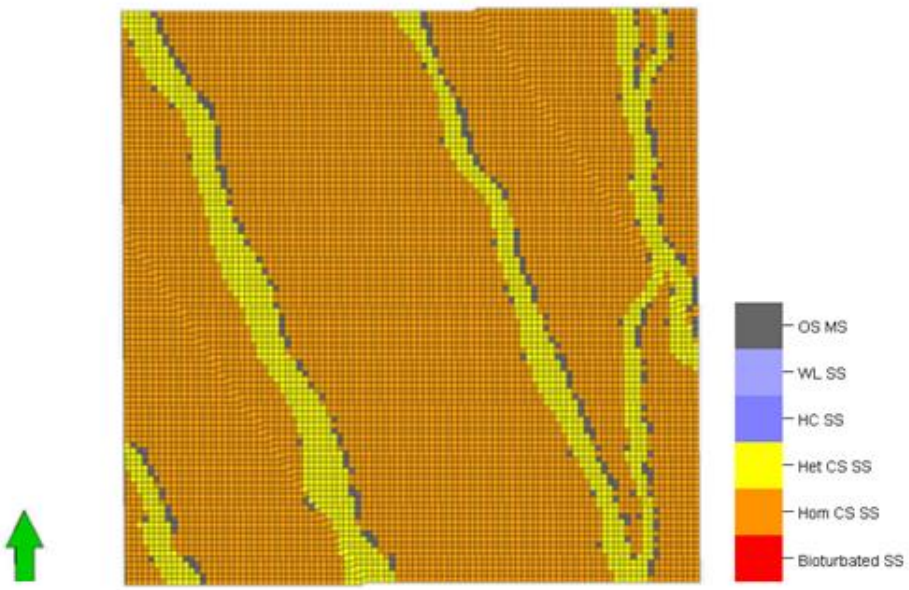

Figure 2.8: Training image for swatchways using adaptive channel object modeling. Yellow = Facies 3; Orange is a background property = Facies 4; Gray = Facies 0. The training image grid is a 30.4 m x 30.4. x 9.1 m. Input parameters are based off of outcrop measurements. The image was taken from Petrel using Gadwin PrintScreen. *add color scale

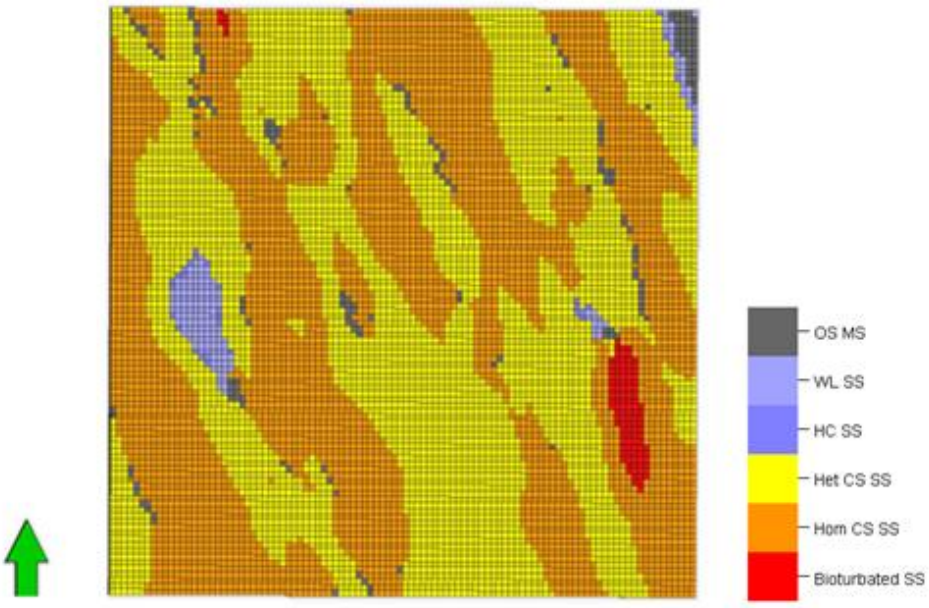

Figure 2.9: Training image representing swatchways cutting through tidal bar elements using the assign value method. The training image grid is a 30.4 m x 30.4. x 9.1 m. The image was taken from Petrel using Gadwin PrintScreen.

Training image two (TI-2) represents a more distal depositional environment of the Sego, characterized by a few isolated tidal bar facies associations and muddy marine background facies associations, with bars oriented parallel to the paleoshoreline and perpendicular to estuarine valley orientations (Fig 2.10). Open marine and shelf facies, including hummocky, cross-stratified sands (F2) and wavy, lenticular sands (F1), dominate. This training image best characterizes the Sego during HST (intervals 1 and 3).

The second-generation Petrel model study area does not encompass the proximal, tidally-influenced fluvial environment of the Sego so a TI was not created for this depositional environment.

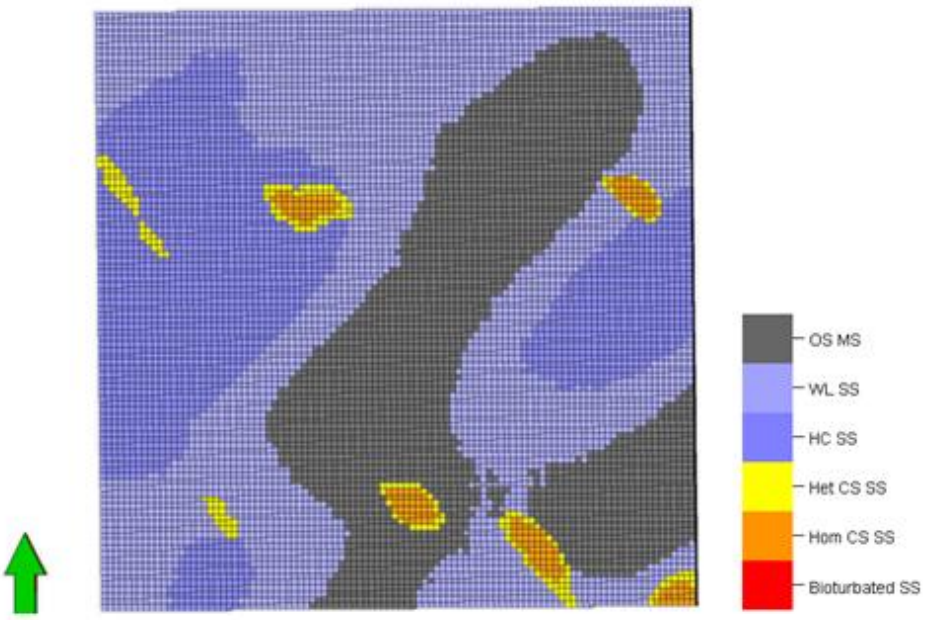

Figure 2.10: Training image two representing the HST of interval 1. The training image grid is a 30.4 m x 30.4. x 9.1 m. Muddy bars are comprised of HC SS (F2) and WL SS (F1) with a OS MS (F0) background property. The image was taken from Petrel using Gadwin PrintScreen.

Secondary Data Conditioning

In addition to existing hard data from well logs and observed outcrop parameters, secondary data integration was used to improve geologic realism within the MPS algorithm. Secondary data, or soft data, introduces indirect, additional data into the model, which is used to further constrain facies simulations (Strebelle, 2006; He et al., 2014). Typical soft data may include seismic data or other geologic observations that function as trends to produce correct facies architectures.

Facies probabilities were generated from upscaled logs through trend modeling for use as volumetric input data to guide vertical and lateral facies distribution through the model (Fig. 2.11). Rotational properties were then created based on observed outcrop orientations to reflect shoreline position and the transition between proximal and distal

depositional settings. Rotational properties were assigned to intervals through the geometrical modeling technique (Fig 2.12).

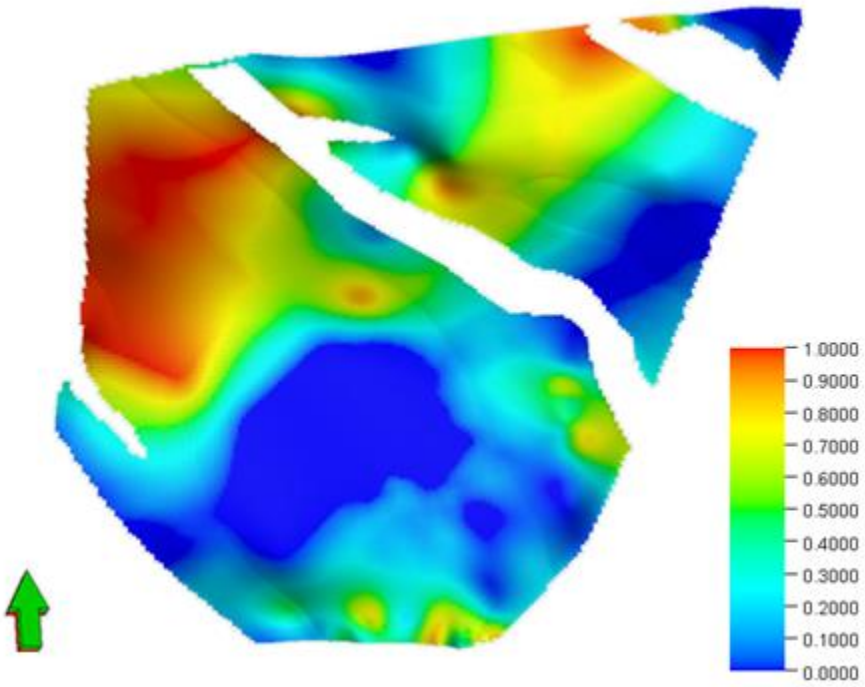

Figure 2.11: Upscaled grid of the probability of homolithic, cross-stratified sands (facies 4) of the FSST, Sego sequence 2 (interval 4). Volumetric facies probabilities were used as a trend modeling input to guide lateral and vertical facies distributions. The vertical exaggeration is set to 15. The grid area is 12.8 km by 10.9 km. The image was taken from Petrel using Gadwin PrintScreen.

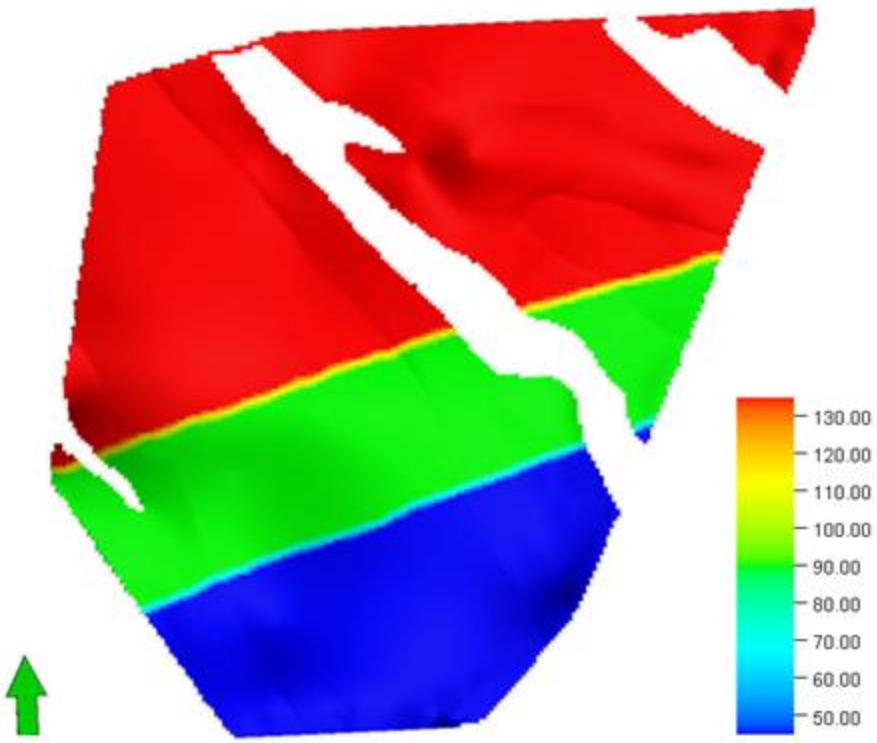

Figure 2.12: The general rotation of facies through the depositional environment delineating shoreline position in the FSST, Sego sequence 2. Red = 135 degrees; Green = 90 degrees; Blue = 45 degrees. The grid area is 12.8 km by 10.9 km. The vertical exaggeration is set to 15. The image was taken from Petrel using Gadwin PrintScreen.

Chapter 3: Petrophysical Modeling and Flow Simulations

PETROPHYSICAL MODELING

Facies distribution models are often viewed as an indicator of algorithm capability in capturing reservoir architecture heterogeneity, but improved petrophysical geostatistical modeling for flow simulations have enhanced model capabilities to capture key reservoir parameters that influence reservoir connectivity. Through petrophysical inputs into reservoir simulation, we can better model dynamic reservoir performance to guide project economics, reduce project risks, and optimize production.

Petrophysical models, including porosity and permeability, were generated based on facies distribution models to create a more comprehensive 3-D reservoir framework of the Sego. Existing porosity and permeability logs from FEDERAL_4-12 were upscaled and value ranges were conditioned to each facies type using a normal distribution (Φ) and log normal distribution (K) based on the previous DecisionSpace model (Appendix C). Mean porosity values were derived from an analysis of the Exxon Carbonera 1 core, while permeability measurements were collected from core plugs using a mini-permameter (Table 3). Values were compared with USGS core plug measurements from the eastern Sego outcrop in Wood and Willis (1999) for accuracy. Petrophysical surfaces were generated using a sequential Gaussian simulation.

	Facies 0	Facies 1	Facies 2	Facies 3	Facies 4	Facies 5
Mean K (md)	Constant (0)	144	175	477	439	326
St Dev	Constant (0)	75.151	3.087	11.653	123.329	1.485
Mean Φ (%)	Constant (0)	16.8	21.2	21.3	21.1	18.4
St Dev	Constant (0)	1.783	3.266	.511	1.175	3.479

Table 3.1: Outcrop permeability data (md) collected from 1.5 cm deep plugs drilled into outcrop then sampled using a mini-permameter (data collected by Willis and Uliana, 1999). Porosity averages and standard deviations were derived from a special analysis of the Carbonera 1 core.

Swatchway features were analyzed as separate petrophysical features by assigning an internal directional trend inside the adaptive channel object to capture high angle lateral accretion deposits (Fig 3.1) and their effect on dynamic flow through small-scale, heterogeneous features.

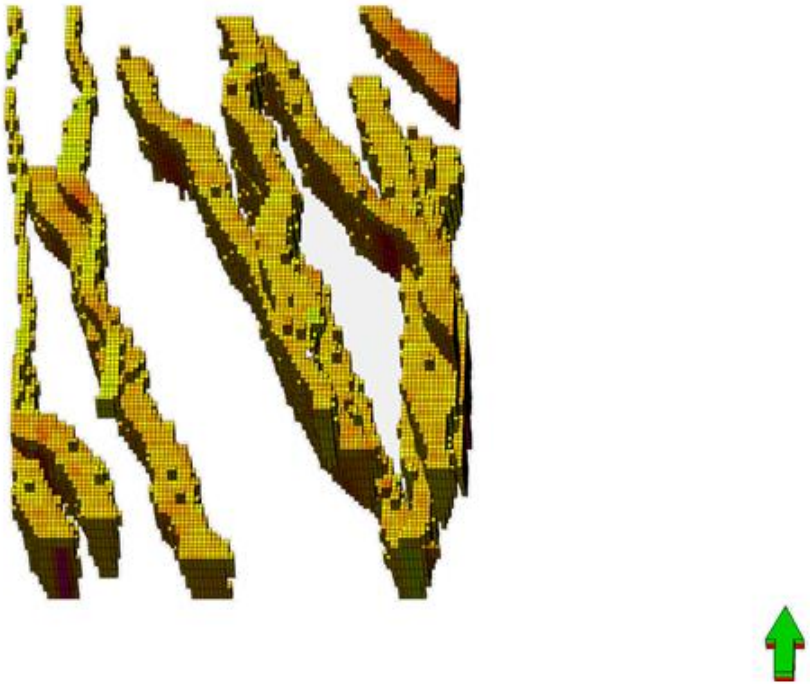

Figure 3.1: Swatchway directional trends in degrees on a scale of 200 degrees to 120 degrees. The training image grid is a 30.4 m x 30.4. x 9.1 m. Dominant directional orientation is 160 degrees (orange) which is consistent with tidal bar orientation. The image was taken from Petrel using Gadwin PrintScreen.

Integration of Shale Anisotropy Estimates on Permeability

Shale length distributions, properties, and localities can significantly affect upscaled vertical permeability, upscaled horizontal permeability, and recovery behavior within reservoirs (Narayanan, 1999; Willis and White, 2000; White et al., 2004). Recent work by Burton and Wood (2011) used LiDAR imaging to capture critical shale character data within confined and unconfined tidal bar elements of the Sego, resulting in the discovery of different effective vertical permeability (K_{ve}) distributions under fluid flow conditions. Using the Monte Carlo simulation method, the study estimated that on average, shorter, more anisotropic shales in confined tidal bars produced a K_v/K_h value of 0.038

and σ=0.027, which were nearly an order of magnitude higher than estimated unconfined values with an average of .004 and σ=0.006.

To test K_{ve} and the ability to image thin shale drapes, vertical permeability data tied to logs was upscaled and modeled as a continuous property using a log normal distribution based off of data collected by Burton (2011). The property calculator was used to determine K_h values using the formula K_h = (unconfined or confined ratio)/Kv and modeled using a sequential Gaussian simulation. Values were then input as volumetric data and tied to tidal bar associations through hierarchical modeling for simulation.

Confined and unconfined bars may occur in each of the five intervals depending on position of the depositional system within the study area. The K_v/K_h value for confined bars was only assigned to the incisional LST of the Sego sequence 2 due to containment within an estuary setting, while K_v/K_h values for larger, unconfined bars were assigned to the remaining FSST and HST intervals based on progradation into abundant accommodation within the system.

Uncertainty Analysis

Uncertainty analyses were conducted through a series of realizations to evaluate the range of uncertain geologic variables within the model. Thirty realization runs were used to determine the arithmetic mean, standard deviation, and P10, P50, P90 for porosity, permeability, and facies distributions to evaluate uncertainty. Definitions for P10, P50, and P90 are as follows: P10 = probability that 10 percent of the realizations will have a specific characteristic; P50 = probability that 50% of the realizations will have a specific characteristic; P90 = probability that 90% of the realizations will have a specific characteristic. Calculations were performed using the inverse cumulative normal distribution function with the computed arithmetic mean and standard deviation to derive

the value of the requested probability percentile (i.e. P10 = InvCumNormal (Mean, Standard Deviation, 0.1). Only 10 MPS realizations were performed to generate P10, P50, and P90 probability maps of facies distributions on each interval due to computational time limitations.

Preliminary Flow Analysis

A preliminary flow analysis was performed to test the flow potential (governed by porosity, permeability and spatial connectivity of facies) across the study area. Facies are defined by their porosity and permeability ratio character, therefore they were binned into discrete categories using the property calculator with high flow potential characterized as a 5 and low flow potential characterized as a 1. Properties given to these categories are as follows: > 2,500 md/% = 5; > 2,000 md/% = 4; > 1,500 md/% = 3; > 1,000 md/% = 2; < 1,000 md/% = 1.

Chapter 4: Results and Discussion

MODELING RESULTS

The results of the MPS models show significant variability in the size, shape, and orientation of tidal bar associations within the resultant 3-D framework built to simulate the Sego stratigraphy. Each MPS simulation was selected to display the range of architectural element distributions. In general, all simulation results honor existing hard data (i.e. well data) and demonstrate observed vertical stacking patterns and lateral facies distributions as observed in outcrop. The Sego sequence 2 LST and FSST results are highlighted in uncertainty analysis and heterogeneity investigations.

Facies Distributions

LST, sego Sequence 2 (upper, Lower Sego)

Interval simulation results from the Sego sequence 2 LST show large scale bars with small amounts of bioturbation in the esuarine transgressive fill (Fig. 4.1). Facies distributions in the Petrel model are visually similar to DecisionSpace results, however, the addition of swatchway incisions in the Petrel simulations narrow confined bar forms making them more elongate to the northwest-southeast. Smaller bar forms are also seen detached from larger bars compared to DecisionSpace results. Continuous shale layers (F0) within swatchways are only evident in a few K layers, but represent a higher proportion of overall interval statistics due to additional representation in TI-1. High amalgamation of tidal bar associations can be seen in the Petrel model throughout the interval.

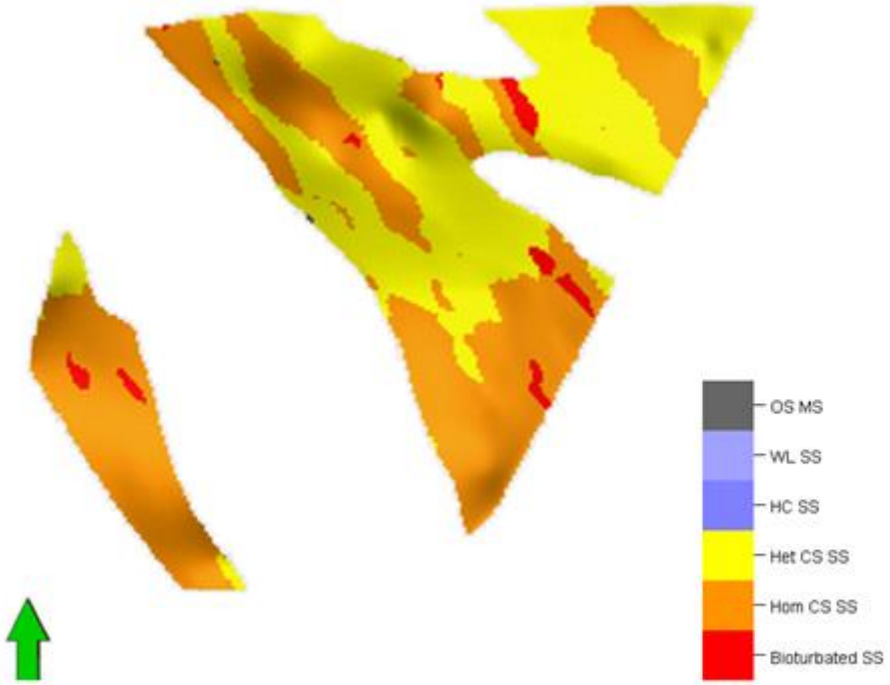

Figure 4.1: MPS realization from the Sego sequence 2 LST. Large bar forms are cut by swatchway incisions, creating thin, elongate bar forms in the transgressive fill. The grid area is 12.8 km by 10.9 km. The image was taken from Petrel using Gadwin PrintScreen.

FSST, Sego sequence 2 (upper, Lower Sego)

Interval simulation results for Sego sequence 2 FSST show a re-orientation of tidal and muddy bar associations through the interpreted shoreline transition (see Fig 2.12; Fig 4.2). Tidal bar associations are larger to the northwest (proximal) and smaller, with greater bioturbation to the southeast near outcrop measurements (distal). Bar forms are more amalgamated in the Petrel model than what was seen in the DecisionSpace model, but such amalgamation is in line with Truncated Gaussian results (Appendix A). Bioturbation percentages are less than observed when using the traditional Truncated Gaussian geostatistical method. Interbar muddy and hummocky, cross-stratified fill is effectively

restricted to more distal sections of the study area and such distribution is consistent with parameters observed in the previous DecisionSpace model.

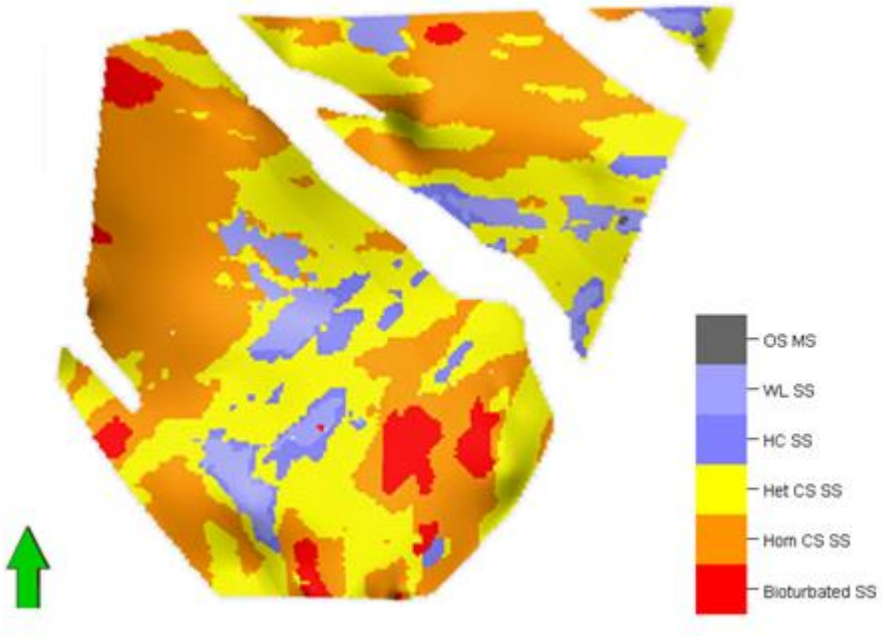

Figure 4.2: MPS realization from the FSST, Sego sequence 2. Bar forms mimic a transitional shoreline by re-orienting across the study area from a NW (proximal) to SE (distal) direction. The grid area is 12.8 km by 10.9 km. The image was taken from Petrel using Gadwin PrintScreen.

HST, Sego sequence 2 (upper, Lower Sego)

Interval simulation results for the Sego 2 HST show small migratory distal bars prograding over large, shore-parallel banks of muddy sands and hummocky, cross-stratified sands (Fig. 4.3). Distal tidal bars, primarily comprised of facies 3, are most common in the NE corner of the study area and are slightly more numerous than observed in the same interval for the DecisionSpace model results. Tidal bars are re-oriented to a 90 degree angle based on additional rotational input data. Some bioturbated Facies 5 caps distal muddy bars and shales near measured outcrop sections in the southeast.

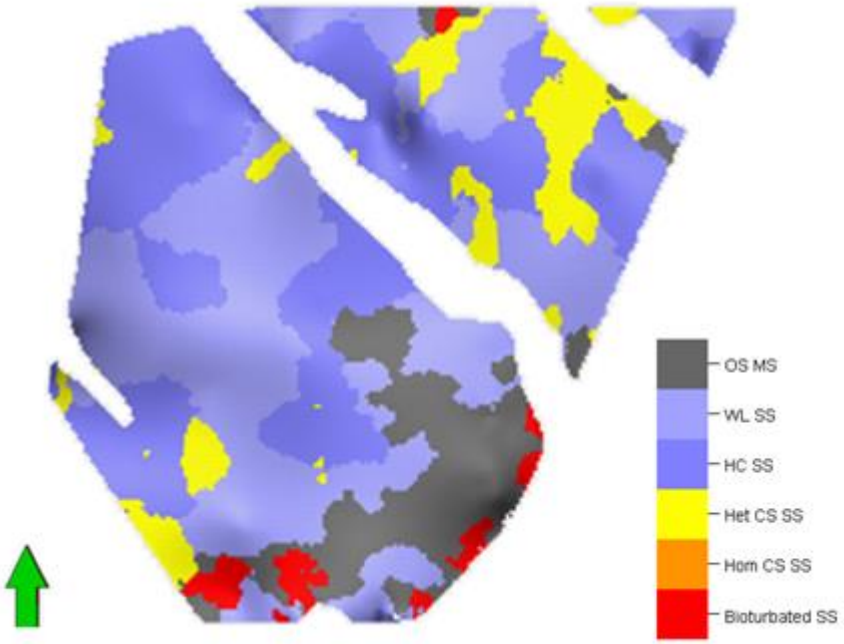

Figure 4.3: MPS realization from the HST, Sego sequence 2. Distal bars are seen prograding over muddy, shoreline parallel bar forms. The grid area is 12.8 km by 10.9 km. The image was taken from Petrel using Gadwin PrintScreen.

FSST, Sego sequence 1 (lower, Lower Sego)

Interval simulation results for the Sego sequence 1 FSST show large scale bar forms with elongate, bioturbated tidal bars aligned in the northwest-southeast direction (Fig 4.4). There are minor, thin packages of muddy fill, but they are not as extensive as within FSST, Sego sequence 2. The Petrel MPS realization shows more amalgamated bar forms, including more extensive bioturbation than the previous DecisonSpace model. A change in shoreline position is evident to the southeast based on a re-orientation of bar forms.

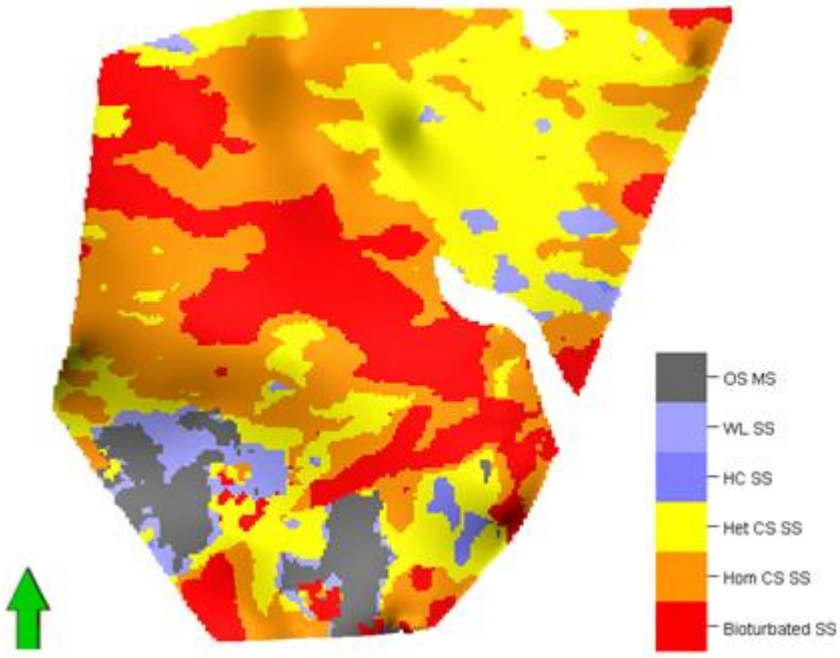

Figure 4.4: MPS realization from the FSST, Sego sequence 1. Large bars forms with extensive bioturbation persist throughout the interval. The grid area is 12.8 km by 10.9 km. The image was taken from Petrel using Gadwin PrintScreen.

HST Buck Tongue

Interval simulation results for the HST Buck Tongue show a small trace of distal tidal bars, but is predominately made up of massive, distal, shoreline parallel muddy bar forms (F1 and F2; gray and dark purple). The MPS simulation result for this interval is extremely similar to the results from the DecisionSpace model.

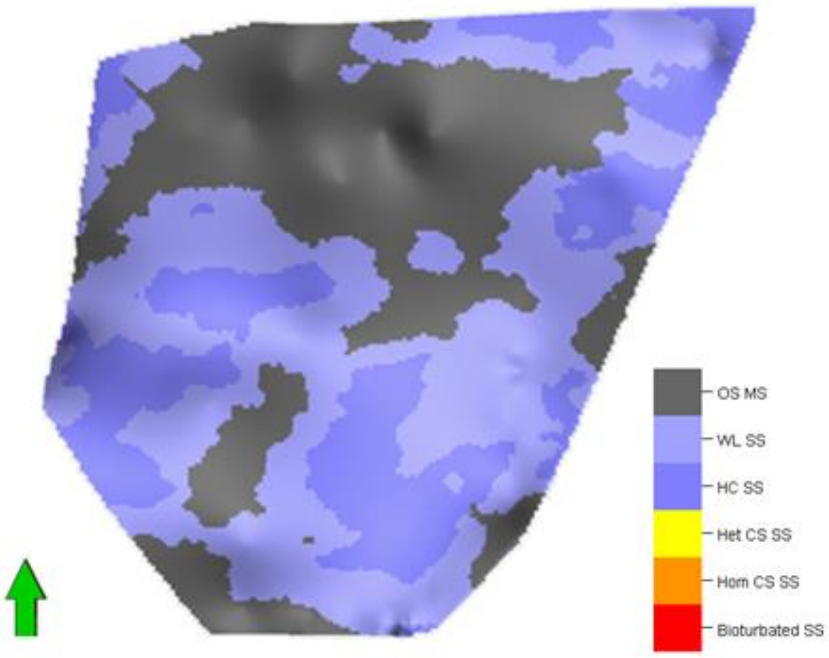

Figure 4.5: MPS realization from the HST Buck Tongue. Distal, muddy bar forms dominate with a predominant orientation of 45 degrees. The grid area is 12.8 km by 10.9 km. The image was taken from Petrel using Gadwin PrintScreen.

Uncertainty Analysis

Petrophysical and Facies Probabilities

Petrophysical model results from uncertainty analyses using P10, P50, and P90 for the Sego sequence two FSST demonstrate a low range of porosity distributions overall (Fig. 4.6). The highest porosity values are found in the heterogenous and homogenous sand facies (F3 and F4), while porosity values are lowest for muddy bars and bioturbated sands, capping tidal bar associations. Lower porosity values realizations are found in the southernmost portions of the study area where environments of deposition were more distal in nature. Visual and statistical comparison of porosity within this interval demonstrates little variation between realizations (Fig 4.6). Permeability has a much wider range of

values across the study area compared to porosity, with high permeability potential closely correlating to facies in both proximal and distal environments of deposition in the study area. Results for facies distributions demonstrate a clear shoreline. While it is possible to find shale in the proximal region of the Sego 2 FSST (blue), heterogeneous and homogenous sands (Facies 3 and 4) are more prevelant. The same is true of finding tidal bars in the more distal environment of deposition regions within the study area.

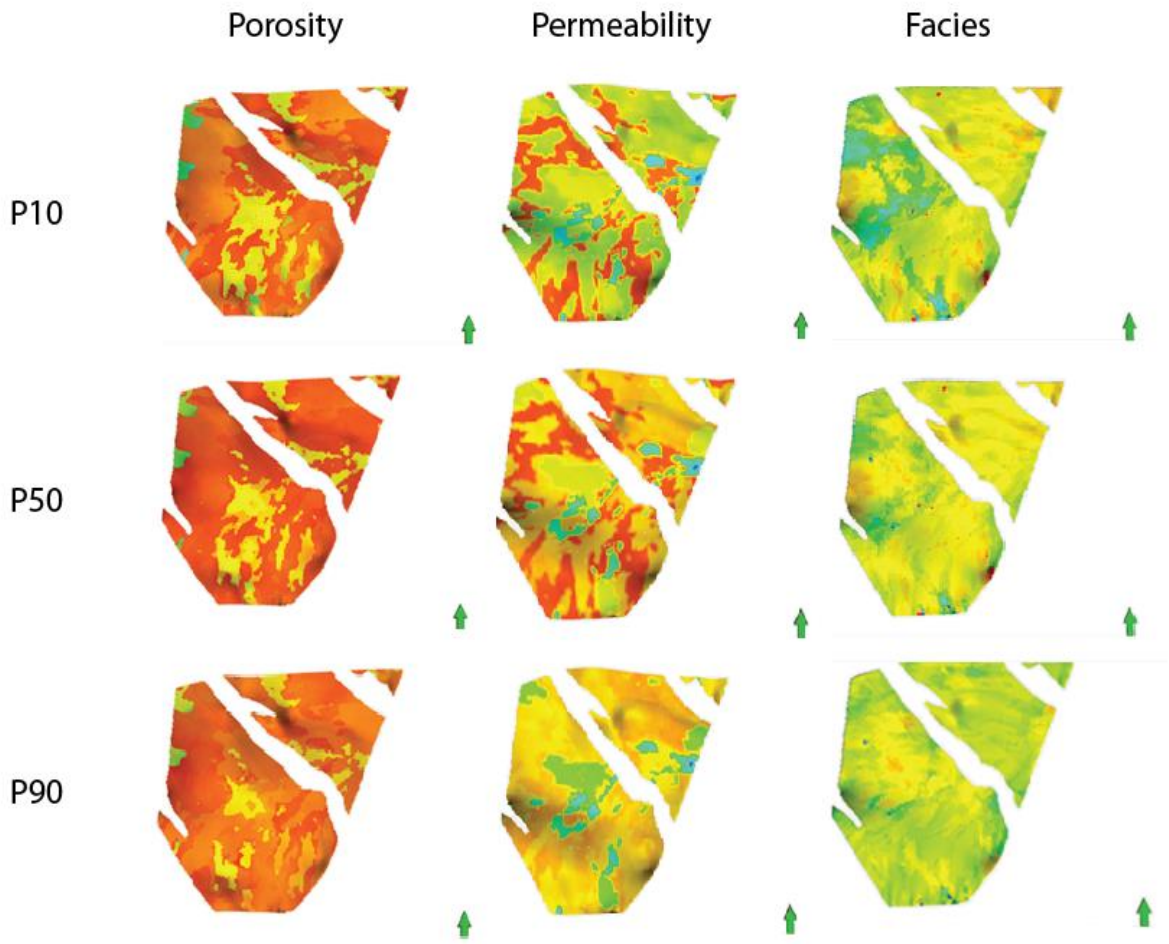

Figure 4.6: P10, P50, P90 of porosity (left), permeability (middle), and facies distribution (right) models from top to bottom for the Sego Sandstone Sequence 2, Falling State System Tract. The porosity scale is from 23% (red) to 0% (blue). Permeability is closely tied to facies distribution. The facies distributions map show the occurrence of facies 5 (red), facies 4 (yellow), facies 3 (orange), facies 2 (purple), facies 1 (blue), and facies 0 (gray). North arrows are shown in green. The study area is approximately 12.8 km by 10.9 km. The image was taken from Petrel using Gadwin PrintScreen.

Fine-scale Heterogeneities

Swatchway features are broadly recognized in modern coastal maps and literature, but are poorly defined and often undocumented in ancient deposits. A swatch, or swatchway is defined by civil engineers as being a flood-tide channel, however, the term is better classified as a passage or channel of water lying between sandbanks or between a sandbank and a shore. The features cut across tidal bars or bar complexes in the Sego and although they are only documented in outcrop (Wood et al., 2011) in the Upper Sego Sandstone, they likely occur broadly as a small-scale, but critical element of these intervals. We chose to model this element as they can be seen cross-cutting tidal bars in the Sego LST 2 in MPS realizations (Fig. 4.7). Stochastic shales within swatchways are accurately represented in the realizations, but are very thin and restricted to upper layers of the Sego LST 2, supported by well data. Additional statistical proportions (from 0.2 to 2 percent) were added to the interval to increase shale influence, but lateral distributions remained relatively unchanged. The addition of directional trends within swatchways does not appear in permeability analyses, but would most likely have an impact in influencing fluid flow direction through these heterogeneous features.

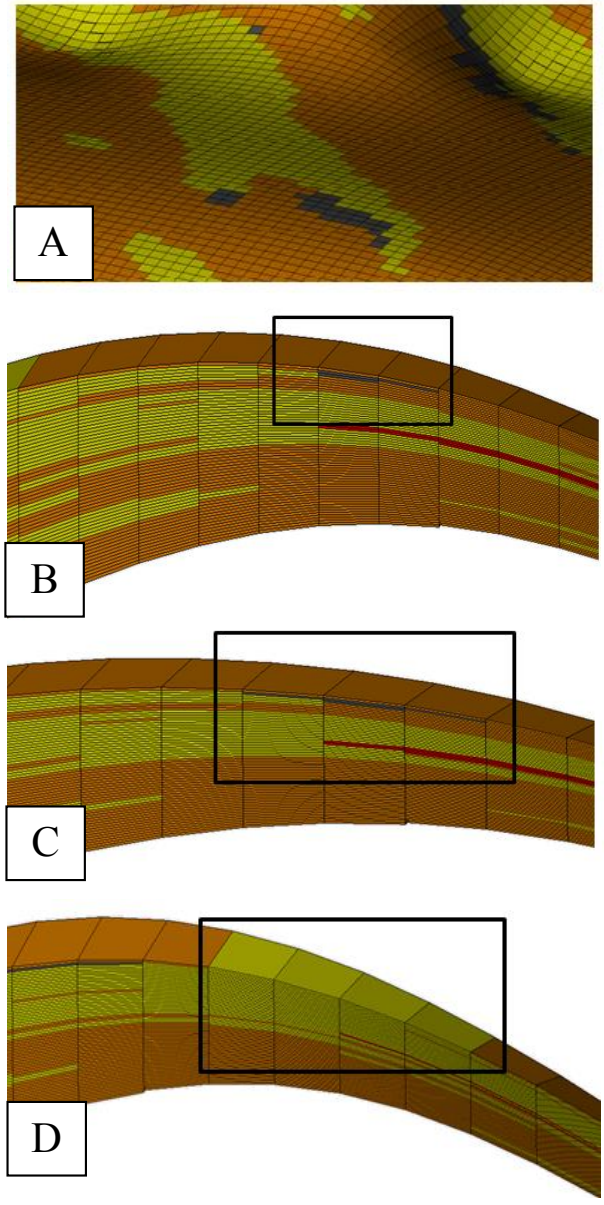

Figure 4.7: Swatchway development through time in the Sego sequence 2 LST. A) Aerial view of stochastic shale distributions within a swatchway. Tidal bars are delineated by homogeneous sands (Facies 3). B) Cross-section of the beginning of a continuous shale layer within a swatchway (J direction). C) Increasing shale distributions in a swatchway through time. Note swatchways are only one layer thick. D) Characteristic heterogeneous sands in the middle of a swatchway cutting through tidal bar facies (orange).

The addition of Kh values to tidal bar associations shows little variability in realizations. Kh values are indicated by other workers (Burton and Wood, 2011) to have little influence on fluid flow within the Sego due to high sand on sand contact. Horizontal barriers for flow are only expected where transmissivity values are low, such as in areas of increased horizon cementation.

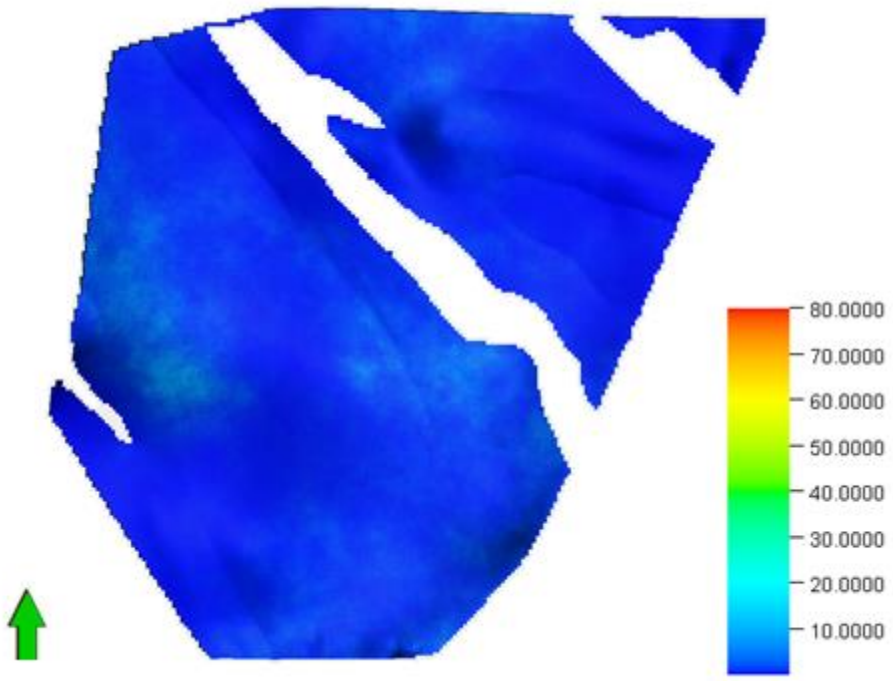

Figure 4.8: Map of the FSST, Sego sequence 2 with Kh values. Kh distributions show little variation in values across the study area. The study area is approximately 12.8 km by 10.9 km. The image was taken from Petrel using Gadwin PrintScreen.

Flow Analysis

The application of the permeability/porosity ratio to test flow conditions produced varying results across facies boundaries. Shales and muddy sands (facies 0, facies 1, and facies 2) near the center of the study area exhibit the lowest flow potential (category 1 or

2), with implications that they would serve as barriers or baffles to flow under simulation conditions (Fig 4.9). Facies 3 shows the greatest connectivity within the interval, while homogeneous sands (facies 4) produce the highest unit values, but show the most variability due to a high standard deviation between permeability values. Bioturbated sands (facies 5) also demonstrate a high variability in values (ranging from 5 to 2), serving as both a conduit and potential baffle to flow. As permeability and porosity attributes are tied to facies, the relationship between facies and value distributions should remain constant. However, this has greater effects considering different facies distributions throughout each of the five Lower Sego intervals. Kh integration into permeability values between confined bars of the Sego sequence 2 LST and the unconfined bars of Sego sequence 2 FSST do not appear to have an effect on estimated flow speeds under this categorical system.

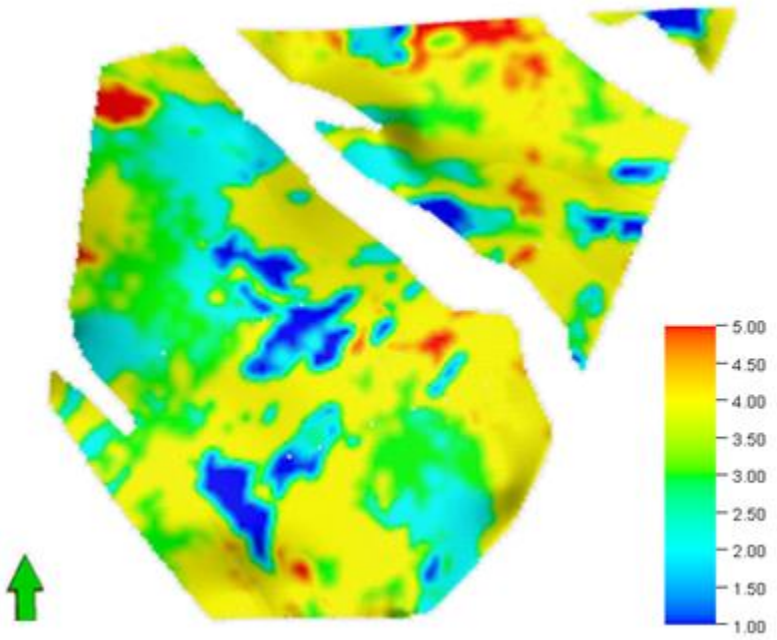

Figure 4.9: Map of the FSST, Sego sequence 2 with estimated flow speeds by category. Flow speeds classified as 5 (red) shows the highest flow potential and flow speeds classified as 1 (blue) show the lowest potential for flow. In this realization, the lowest values are attributed to distal muddy sandbanks (facies 1 and 2) while the highest values attributed to homogenous sands (facies 4) or bioturbated layers (facies 5). The study area is approximately 12.8 km by 10.9 km. The image was taken from Petrel using Gadwin PrintScreen.

DISCUSSION

Outcrop-to-subsurface geomodeling provides modelers with deterministic and geostatistical spatial distributions of properties that result in a greater understanding of geologic concepts and crtitical insight into identifying the most influential factors affecting flow behavior. The previous sections discuss the enhancement of a static reservoir model to capture key facies proportions and distributions as part of larger architectural elements to capture realistic heterogeneities in complex geologic systems. This section outlines a comparison of the key differences between results from the first-generation DecisionSpace model and the further conditioned second-generation Petrel model.

Truncated Gaussian Method

The Truncated Gaussian geostatistical method used in the second-generation Petrel model produced similar facies relationships in lateral variability and vertical stacking as the first-generation, DecisionSpace model. In addition, known tidal bar lithotypes were preserved, however multiple lithotypes as defined by the DecisionSpace software's Plural-Gaussian methods were not able to be recreated within the same model realization using the Petrel software. The Truncated Gaussian approach allows the user to simulate one or several continuous Gaussian fields and to truncate them in order to produce a categorical variable (Isaaks, 1984; Matheron, 1987; Mariethoz et al., 2008). However, Plural-Gaussian holds the advantage of integrating multiple geological concepts through the *lithotype rule* (Le Loc'h and Galli, 1994) to establish accurate facies distributions within a high-resolution, stochastic model framework. These relationships were reproduced in the Truncated Gaussian Petrel software generated model using vertical proportion curves and volumetric facies probabilities from data analysis, but results often overestimated facies proportions, especially bioturbation percentages. While both techniques were successful in defining and honoring facies relationships, they yielded realizations that did not fully capture architectural element heterogeneity, in the DecisionSpace model, thus leading to the research question of how might a Petrel model, using the more advanced MPFS, show advantages to the older model.

MPFS Model

Facies Distributions

The MPFS Petrel model addressed several limitations and recommendations of the first-generation DecisionSpace model, including the modeler's preference to manually

generate a representative pattern model (in this study a TI) to better guide facies distribution simulations and the desire for more user-defined parameters within the modeling process. The use of secondary data, such as expected facies probabilities and rotation of architectural elements within each interval, enhanced model resolution and allowed for greater honoring of depositional complexities across the study area.

Building a successful geostatistical MPS model relied on several key factors tied to TI generation including the initial deterministic outcrop data to guide variograms, the integration of lithologic proportions directly into TIs, and maintenance of complex facies relationships within facies associations. Hierarchical modeling through a nested approach was an essential tool to capture fine-scale features and heterogeneity such as swatchways and K_v/K_h integration within tidal bar facies associations. Resolution of internal heterogeneity proved difficult as many of the finer scale heterogeneities such as continuous shale beds on the cm scale, could not be successfully represented in the k direction when looking at a kilometer scale study area.

The most important feature to consider in TI generation is facies proportions and the application of similar facies proportioned TIs to adjacent regions. An initial attempt to represent tidal bar associations through object modeling in Petrel failed due to the inability to capture critical facies assemblage relationships, thus the Truncated Gaussian technique was deemed preferable for facies population within TIs. While not as ergodic and stationary as object-modeled features, pattern tests of TIs using truncated Gaussian showed successful replication of bar forms based on the ratio of variogram parameters. This was not surprising as Gaussian simulation is based on an elliptical distribution, which coincides with bar form shape. The selection of three multi-grids was a highly influential variable in preserving these values and transferring deterministic geologic characteristics for input into MPS. As training images are conceptual and do not have to be conditioned to hard data,

complex interactions between facies may be represented in Petrel without the limitations of simple object-modeling.

The use of secondary data to condition MPS models was successful in providing additional interpreted constraints to influence primary model results. Tidal bar forms adhered to rotational inputs and facies probability trends, mimicking transitional shorelines under transgressive-regressive conditions by restricting proximal and distal facies distributions. While the use of zonation is a critical concept for characterizing complex depositional transitions, the upscaled log data did not support the degree of user-defined shoreline transition within the study area. This was not surprising based on the relatively small study area compared to common kilometer spatial scales of gradational shoreline transitions.

Fine-scale Heterogeneities

Shale proportions were increased within the swatchway TI to account for the presence of more continuous shale layers within the Sego LST 2. However, the influence of shales in general facies distributions remained minimal due to low overall proportion statistics. It is likely that very thin shale units (on the cm scale) within swatchway features were lost through averaging in a general upscaling of facies associations to the larger study area grid. This argues that a higher resolution grid within a smaller study area is required to accurately capture very fine-scale features and their impact on reservoir fluid flow.

In a permeability analysis of Sego LST 2, the lack of large scale, low permeability shale continuity as a function of depth was apparent (Fig 4.7). Changes in permeability distributions between heterogeneous sands (F3) and the surrounding tidal bar associations were minimal, which would encourage connectivity between the main body of swatchways

and surrounding tidal bar associations, effectively limiting low permeability units from acting as strong baffles to flow.

While confined and unconfined tidal bars are composed of similar facies, with similar measured porosity and permeability, the difference in Kve distributions is significant to capture in modeling internal heterogeneity within architectural elements. Models results from the Sego sequence 2 LST demonstrate shorter, more amalgamated confined tidal bars, which enhance connectivity between flow units.

Uncertainty Analysis

Information from uncertainty analysis is critical to integrate into any modeling process as it provides an understanding of reservoir behavior for accurate assessment and reservoir performance prediction. Porosity and permeability uncertainty analyses from the FSST Sego 2 indicate that any of the porosity realizations could effectively be used to classify porosity distribution within the interval framework as there is relatively little variation between outcomes; i.e. very little uncertainty in the model. As porosity and permeability values are conditioned to facies distributions, capturing accurate vertical and lateral heterogeneity is the most significant control in classifying risks within the Sego.

Implications for Flow Models

Based on preliminary flow simulations, tidal bars within the estuarine valley fill exhibited cross-boundary flow, with fluid from injectors able to avoid baffles and to effectively flow in three dimensions. The heterolithic nature of the estuarine valley fill contributed to an increased flow response in areas of higher tidal bar amalgamation and less where bars become separated by thicker shale units. Tidal bar associations in the model also demonstrated positive pressure even when not directly connected to the valley fill. As permeability generally increases with grain size, we would expect flow to direct

towards higher permeability units such as the heterogeneous (F3) and homogenous sands (F4) and divert around low low permeability shales (F0). A complete 3-D reservoir framework was generated for the creation of a volumetric model to test second-generation flow results.

Relevance to Petroleum Systems

Geostatistical simulations in static geomodeling are preferable to simple interpolation methods as statistical methods more successfully capture the heterogeneous nature of reservoirs and thus provide a more accurate estimate of both hydrocarbon reserve and production behavior expectation. Generating realistic facies distributions through geostatistics is critical to understanding petroleum systems, as rock properties are often linked to facies definitions. Such an approach of linkage between rock properties and realistic facies distribution, rather than simple averaging of properties across the entirety of a reservoir, is more desirable in the modeling process. Simulated models also help to guide a comprehensive development plan of a field, optimize production, and enhance performance predictions, which affect revenue and capital allocation by avoiding costs associated with exploration and development of heterogeneous reservoirs. As computing technology and geostatistical modeling methods continue to improve, reservoir simulations will become an increasingly critical tool in evaluating reservoir strategies and quantifying economic uncertainty (Begg et al., 2001). Simulations must be applied with care, however, as analogous systems with similar depositional architectures may contain differences in fluid and rock properties, which impact flow behavior (White et al., 2004).

CONCLUSIONS

The research presented here accomplishes three goals. These include: 1. The exploration of MPS as an improved geostatistical approach for modeling heterogeneous,

tidally-influenced systems, 2. to investigate the role of architectural elements as framework geometries for impacting fluid flow, with specific attention to fine-scale, heterogeneous features such as swatchways, tidal channels, bioturbated layers and shale distributions within different bar morphologies, and 3. To comment on the capabilities and results of a second-generation, Petrel-based MPS model over a first-generation DecisionSpace model.

The MPS geostatistical method was integrated into the model through Petrel's MPFS algorithm and applied to model intervals through the use of training images and secondary data. Architectural element distributions were explored through a series of MPS training images tied to proximal and distal depositional environments of the Sego, which honored upscaled statistical proportions and guided facies distributions. The use of Truncated Gaussian within training image patterns proved critical in preserving element geometries and facies associations within each interval of the Petrel model. Outcomes showed that additional secondary attributes (i.e. rotation, facies probabilities, and zonation) honored greater depositional complexity across the study area than the original DecisionSpace model, through Petrel's ability to capture regressive-transgressive shorelines.

The MPFS method allowed for the successful inclusion of fine-scale, heterogeneous features such as swatchways and K_v/K_h within user-defined training images hinged on a nested modeling approach. Swatchway heterogeneity was specifically well defined in model results, where shale distributions within swatchways could be seen cutting through tidal bar associations. However, model results of heterogeneities also demonstrate the need for an even higher resolution, fine-scale model to better capture the level of detail required to accurately characterize these features.

Through better conditioning of model parameters and the integration of fine-scale features, the Petrel-based MPS model effectively addressed the limitations of the first-

generation DecisionSpace model and should be considered for addressing complexities in heterogeneous depositional systems.

Limitations and Future Work

While MPS provides the latest invaluable tool in producing high-order spatial statistics for geologic concepts, the method is not without limitations in capturing system heterogeneity. As the use of MPS relies on the discrete geologic understanding of the study area by the geomodeler through a user-defined training image, conceptual and parametric errors are possible. Despite the fact that such tools as MPS exist, insufficient data and parameterization difficulties in the construction of detailed, geologically accurate training images often favors the use of more traditional geostatistical methods (i.e. Plural-Gaussian) to model spatial continuities (Mariethoz and Kelly, 2011). These difficulties are most likely a contributing factor to an overall lack of widespread MPS adoption by industry as a preferred method for modeling complex reservoir systems.

Limitations also exist within the data of the second-generation model. While outcrop measurements provided good deterministic input data for spatially modeling tidal bar associations, they provided only a sample of the subsurface and may not fully characterize the heterogeneity and complexity of architectural elements in the Sego. More detailed data, such as 3D seismic, could be integrated to provide more model parameters and would allow for further characterization of the Sego subsurface in the study area. Flow analysis could have been better guided by additional porosity and permeability data as well as through the use of production data with associated subsurface wells to adjust model input parameters. Given more continuous property data (i.e. Φ ,K, Sw), I would have also generated discrete properties and displayed them in a vertical proportion curve window to analyze potential trends for greater petrophysical conditioning of the model.

Given greater time, more complex geostatistical theories in conjuction with Petrel's MPFS would have been explored. Finally, only tidally-influenced environments are explored in this research, so it is unclear how the suggested Petrel modeling workflow will vary based on other depositional systems.

The limitations of this study provide a starting point for future work:

1. To generate additional MPS capabilities that allow for greater integration of non-stationary images to improve reproducible geological heterogeneities at multiple scales (Arpat and Caers, 2004; Zhang et al., 2004).
2. Increased MPS capabilities to extract specific features such as "tidal bars" from images and obtain statistics and input parameters for more accurate object modeling.
3. Increase user-defined parameters that allow for even greater data integration to obtain more accurate and realistic models
4. Enhanced methods for combining geostatistical methodology with flow simulations

Appendices

APPENDIX A: DECISIONSPACE MODELING RESULTS

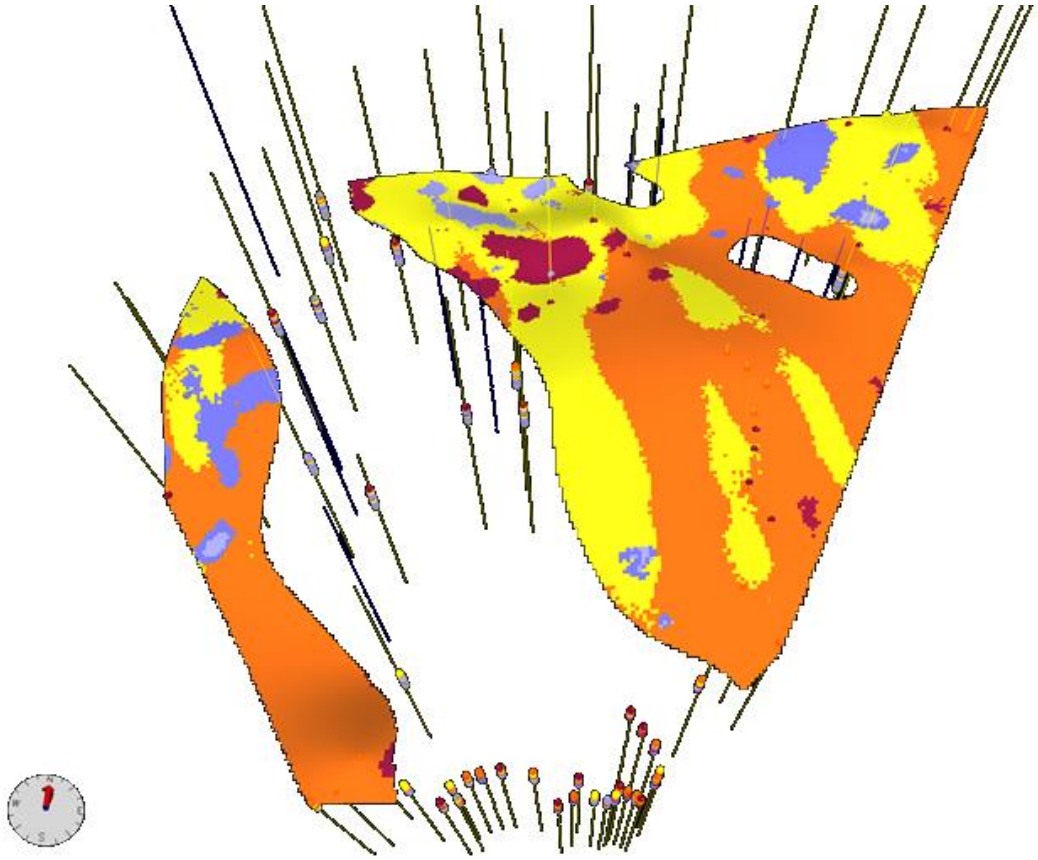

Figure A.1: Example Plural-Gaussian realization of the LST, Sego sequence 2 from the preliminary DecisionSpace model. The realization exhibits large bar forms in the estuarine valley fill (yellow), with some interbar muddy fill (purple). However, these muddy facies 1 and 2 are meant to be open marine shelf facies and are not well constrained, often appearing in the middle of estuarine bars. In addition, the bioturbated facies (maroon) are not well constrained, appearing randomly distributed.

APPENDIX B: TRUNCATED GAUSSIAN MODELING RESULTS

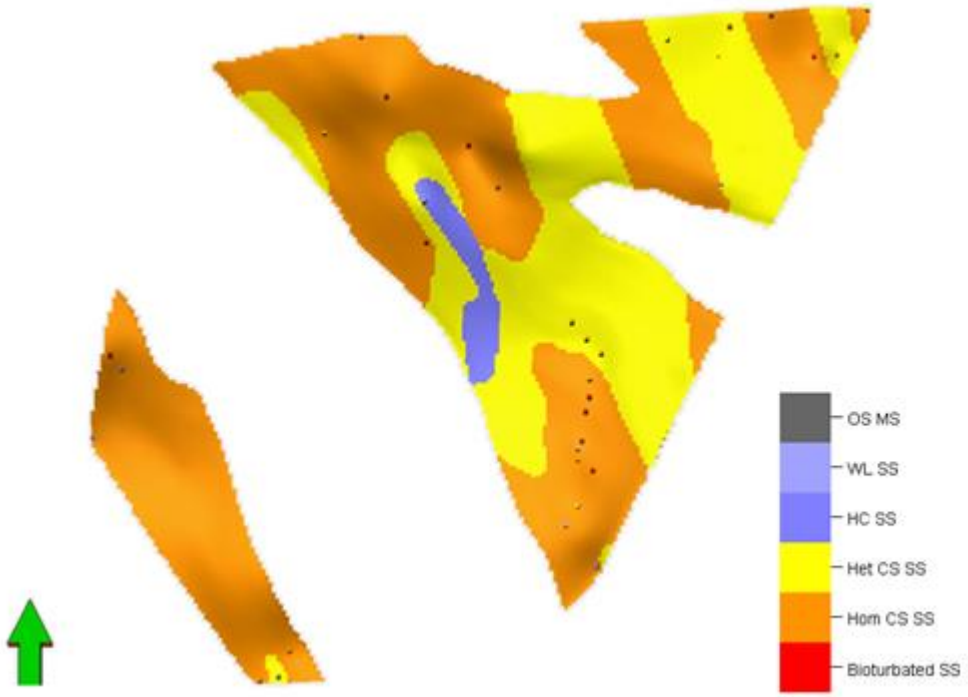

Figure B.1: Truncated Gaussian realization of the LST, Sego sequence 2. The realization exhibits large bar forms in the estuarine valley fill, with some interbar muddy fill. The grid area is 12.8 km by 10.9 km. Vertical exaggeration is set to 15.

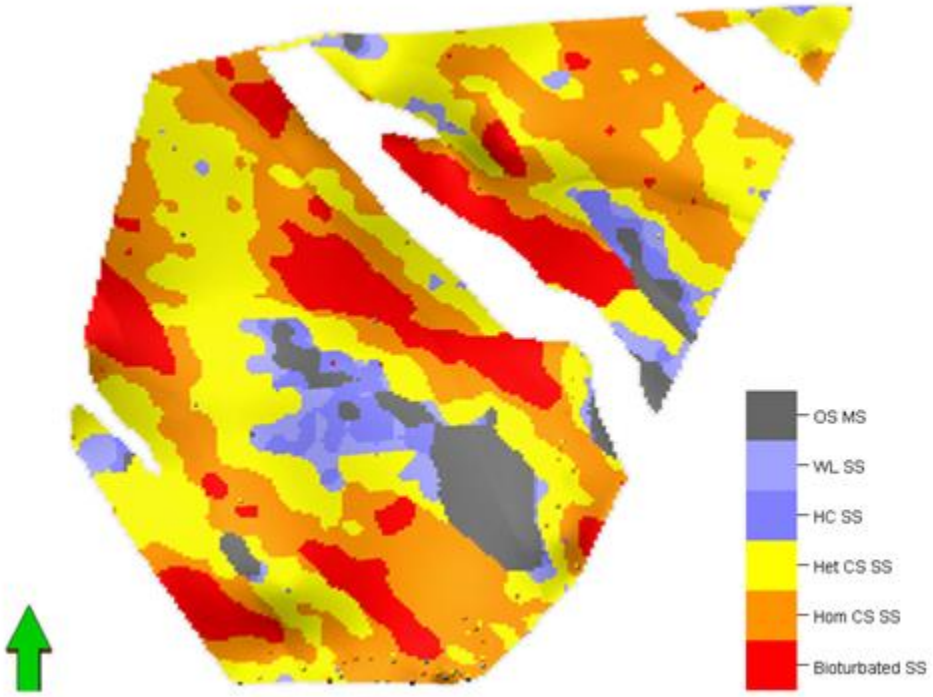

Figure B.2: Truncated Gaussian realization of the FSST, Sego sequence 2. The interval consists of smaller tidal bars than in the FSST, Sego sequence 1, with thick packages of interbar muddy facies. In this realization, the interbar muddy facies (purple and gray) is truly distributed in elongate form between the large barforms (orange and yellow). In addition, the bioturbated facies 5 (red) is much better distributed in homogeneously sandy, bar tops. The grid area is 12.8 km by 10.9 km. Vertical exaggeration is set to 15.

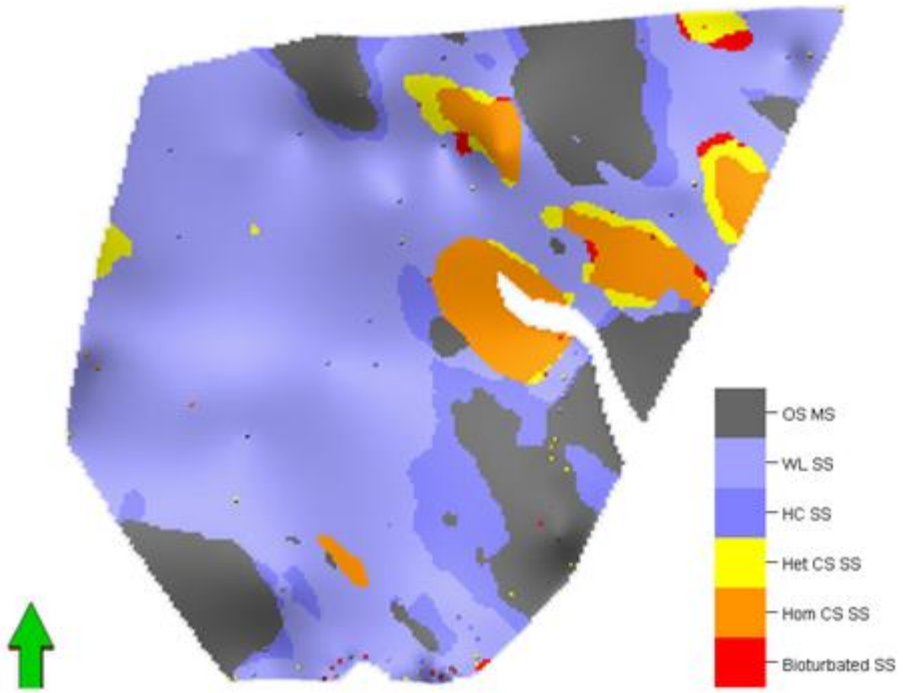

Figure B.3: Truncated Gaussian realization of the HST, Sego sequence 2. This interval is characterized by small, distal tidal bars with small amounts of bioturbation. Bars show heterolithic facies (yellow) along the margins and flanks of bars. These bars are isolated in a shelf system of hummocky, cross-stratified sands and muddy, silty shelf deposits. The grid area is 12.8 km by 10.9 km. Vertical exaggeration is set to 15.

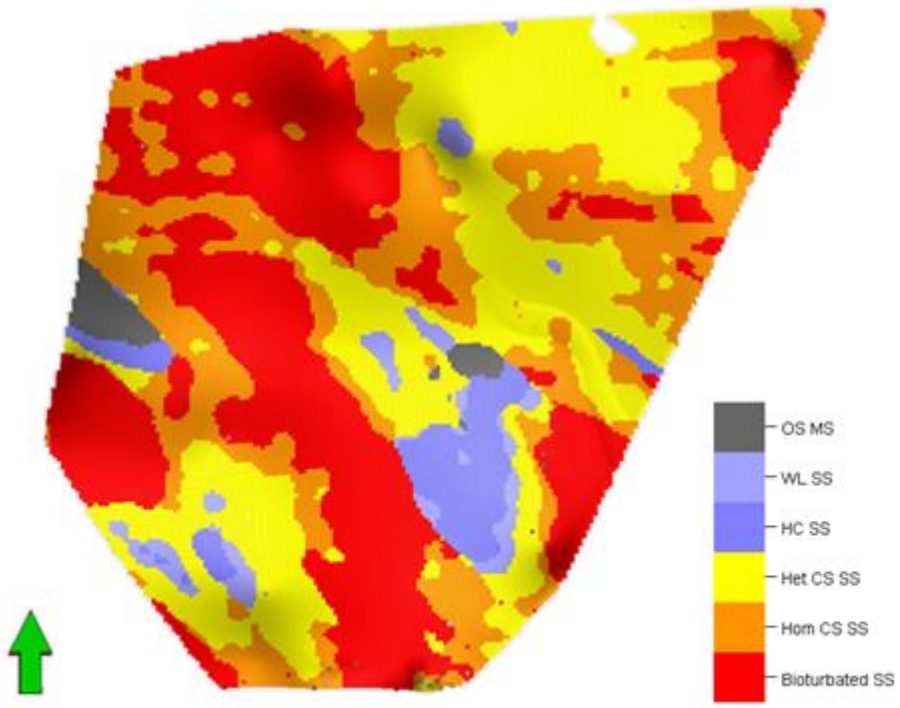

Figure B.4: Truncated Gaussian realization of the FSST, Sego sequence 1. Tidal bars in this interval are larger than in FSST Sego sequence 2, with more extensive bioturbation. There is limited muddy interbar fill between tidal bar forms. These characteristics belie the nature of the falling-stage 1 as more sheet like in nature, being early in the fall cycle. This system is more marine than the later FSST 2, thus increased bioturbation. The grid area is 12.8 km by 10.9 km. Vertical exaggeration is set to 15.

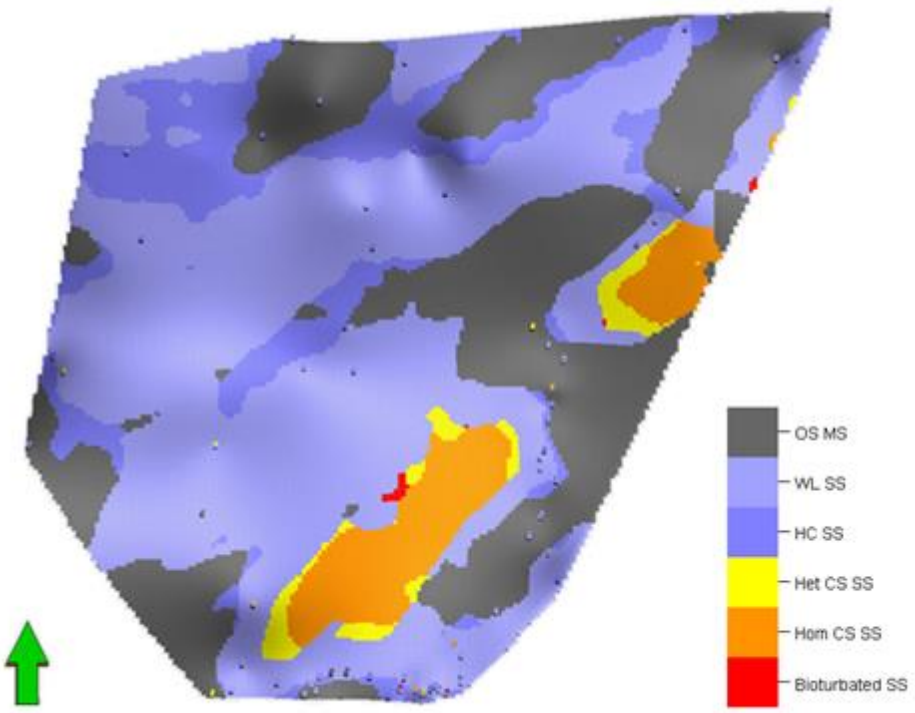

Figure B.5: Truncated Gaussian realization of the HST Buck Tongue. Small tidal bars exist in the distal direction, but the interval primarily consists of shoreline parallel muddy bar forms. Bar form orientation is a function of dominance of marine wave and offshore forces remolding offshore sands parallel to the shoreline. The grid area is 12.8 km by 10.9 km. Vertical exaggeration is set to 15.

APPENDIX C: POROSITY AND PERMEABILITY DISTRIBUTION METHODS

	Facies 0	Facies 1	Facies 2	Facies 3	Facies 4	Facies 5
Interval 5	Constant (0)	Normal (20, 1)	Normal (22, 1)	Normal (23, 0.25)	Normal (23, 1)	Normal (20.5, 0.5)
Interval 4	Constant (0)	Normal (20, 1)	Normal (22, 1.5)	Normal (23, 0.25)	Normal (23, 1)	Normal (20.5, 0.5)
Interval 3	Constant (0)	Normal (20, 1)	Normal (22, 1.5)	Normal (23, 0.25)	Normal (23, 1.5)	Normal (20.5, 0.5)
Interval 2	Constant (0)	Normal (20, 1)	Normal (22, 1.5)	Normal (23, 0.25)	Normal (23, 1)	Normal (20.5, 0.5)
Interval 1	Constant (0)	Normal (20, 1)	Normal (22, 1.5)	Normal (23, 0.25)	Normal (23, 1.5)	Normal (20.5, 0.5)

Table C.1: Range of porosity values and distribution method by interval used in petrophysical modeling (after Dunlap et al., 2012). Intervals were defined previously under the 3-D Grid construction section.

	Facies 0	Facies 1	Facies 2	Facies 3	Facies 4	Facies 5
Interval 5	Constant (0)	Lognormal (300, 100)	Lognormal (300, 100)	Lognormal (600, 200)	Lognormal (600, 200)	Lognormal (500, 250)
Interval 4	Constant (0)	Lognormal (300, 100)	Lognormal (300, 100)	Lognormal (600, 200)	Lognormal (600, 200)	Lognormal (500, 250)
Interval 3	Constant (0)	Lognormal (300, 100)	Lognormal (300, 100)	Lognormal (600, 200)	Lognormal (600, 200)	Lognormal (500, 250)
Interval 2	Constant (0)	Lognormal (300, 100)	Lognormal (300, 100)	Lognormal (600, 200)	Lognormal (600, 200)	Lognormal (500, 250)
Interval 1	Constant (0)	Lognormal (300, 100)	Lognormal (300, 100)	Lognormal (600, 200)	Lognormal (600, 200)	Lognormal (500, 250)

Table C.2: Range of permeability values and distribution method by interval used in petrophysical modeling (after Dunlap et al., 2012). Values are measured in millidarcy (md). Intervals were defined previously under the 3-D Grid construction section. The lognormal distribution is based off White et al. (2004).

APPENDIX D: GLOSSARY OF TERMS

Kriging

A geostatistical technique, which interpolates concentration values for locations between sampling points.

Multiple-point Statistics (MPS)

A facies modeling technique, which interpolates using multiple points instead of conventional variogram-based techniques founded on bi-point statistics. MPS offers another way to model complex and heterogeneous geological environments through the use of a training image (see Training Image).

Realization

In probability and statistics, it is the value of the outcome that is observed.

Simulation

The imitative representation of the functioning of one system or process by means of the functioning of another. Geostatistical simulations produce realizations (see Realization).

Stochastic simulation

The generation of multiple equally probable images of the variable; also employs semivariogram model.

Training Image

A pattern-based image used in Multiple-point statistics that describes the geometrical characteristic of facies to be modelled.

Variogram

A function that quantifies the spatial correlation between two sampling points. In order to apply kriging to a data set, it is necessary to model the variogram.

References

Arpat, G. B., 2005, Sequential simulation with patterns: Stanford University, pp. 1-166.

Arpat, B., and Caers, J., 2007, Conditional simulation with patterns, Mathematical Geology, vol. 39, no. 2, pp. 177-203.

Begg, S. H., Bratvold, R. B., and Campbell, J. M., 2001, Improving investment decisions using a stochastic integrated asset model: 2001 Society of Petroleum Engineers Annual Technical Conference and Exhibition, New Orleans, September 30-October 3, SPE Paper no. 71414, CD-ROM, p. 16.

Burton, D., 2011, Geologically-based permeability anisotropy estimates for tidally-influenced reservoir analogs using LIDAR-derived, quantitative shale character data: The University of Texas at Austin, pp. 1-220.

Burton, D., and Wood, L.J., 2011, Quantitative shale characterization of the tidally influenced Sego Sandstone, AAPG Bulletin, v. 95, no. 8, pp. 1207-1226.

Caers, J., and Zhang, T., 2002, Multiple-point geostatistics: A quantitative vehicle for integrating geologic analogs into multiple reservoir models, *in* Integration of outcrop and modern analogs in reservoir modeling: AAPG Memoir 80, pp. 383-394.

Caers, J., and Scheidt, C., 2011, Integration of engineering and geological uncertainty for reservoir performance prediction using a distance-based approach, *in* Y. Z. Ma and P. R. La Pointe, eds, Uncertainty analysis of reservoir modeling: AAPG Memoir 96, pp. 191-202.

Cronkite-Ratcliff, C., Phelps, G. A., and Boucher, A., 2012, A multiple-point geostatistical method for characterizing uncertainty of subsurface alluvial units and its effects on flow and transport: U.S. Geological Survey Open-File Report 2012-1065, p. 24.

Dalrymple, R. W., and Rhodes, R. N., 1995, Estuarine dunes and barforms, *in* Geomorphology and Sedimentology of Estuaries, ed.: Developments in Sedimentology, v. 53, Amsterdam, Elsevier, pp. 359-422.

Dalrymple, R. W., and Choi, K. S., 2007, Morphologic and facies trends through the fluvial-marine transition in tide-dominated depositional systems: A schematic framework for environmental and sequence-stratigraphic interpretation, ScienceDirect, Earth-Science Reviews 81, pp. 135-174.

Deveugle, P. E. K., Jackson, M. D., Hampson, G. J., Steward, J., Clough, M. D., Ehighebolo, T., Farrell, M. E., Calvert, C. S., and Miller, J. K., 2013, A comparative study of reservoir modeling techniques and their impact on predicted performance of fluvial-dominated deltaic reservoirs: AAPG Bulletin, v. 98, no. 4, pp. 729-763.

Dunlap, D. B., Burton, D., and Wood, L. J., 2010, Reservoir Modeling of Highly Heterolithic Tidal Shoreline Deposits in the Sego Sandstone, Utah; Translating Detailed Outcrop Knoweldge to Subsurface Understanding of Flow in Stratigraphically Complex Systems, AAPG Poster.

Erdmann, C. E., 1934, The Book Cliffs coal field in Garfield and Mesa Counties, Colorado: U.S. Geological Survey Bulletin, 851, p. 150.

Fisher, W. L., 1936, Mineral sin the Bates limestone, Lewiston, Maine: American Mineralogist, v. 21, no. 5, pp. 321-326.

Fisher, D. J., Erdmann, C. E., and Reeside, J. B., Jr., 1960, Cretaceous and Tertiary formations of the Book Cliffs, Carbon, Emery, and Grand Counties, Utah, and Garfield and Mesa Counties, Colorado: U.S. Geological Survey Professional Paper, 332, p. 80.

Franczyk, K. J., 1989, Depositional controls on the late Campanian Sego Sandstone and implications for associated coal-forming environments in the Uinta and Piceance basins, IN Evolution of sedimentary basins; Uinta and Piceance basins: U.S. Geological Survey Bulletin, 1787-F, pp. F1-F17.

Franczyk, Kl. J., Pitman, J. K. and Nichols, D. J., 1990, Sedimentology, mineralogy, palynology, and depositional history of some uppermost Cretaceous and lowermost Tertiary rocks along the Utah Book and Roan cliffs east of the Green River, IN Evolution of sedimentary basins; Uinta and Piceance basins: U.S. Geological Survey Bulletin, 1787-N, pp. N1-N27.

Galloway, W. E., 1989, Genetic stratigraphic sequences in basin analysis; II, Application to Northwest Gulf of Mexcio Cenozoic basin: AAPG Bulletin, v. 73, pp. 125-142.

Guardiano, F., and Srivastava, M., 1993, Multivariate geostatistics, beyond bivariate moments, *in* Soares, A. ed., Geostatistics Troia '92: v. 1., pp. 133-144.

He, X. L., Sonnenborg, T. O., Jorgensen, F., and Jensen, K. H., 2014, The effect of training image and secondary data integration with multiple-point geostatistics in groundwater modeling, Hydrol. Earth Syst. Scie, v. 18, pp. 2943-2954.

Hettinger, R. D., Kirchbaum, M. A., 2003, Stratigraphy of the Upper Cretaceous Mancos Shale (upper part) and Mesaverde Group in the southern part of the Unita and Piceance Basins, Utah and Colorado, *in* Kirschbaum, M. A., ed., U. S. Geological Survey Digital Data Series: United States, U. S. Geological Survey: Reston, VA, United States.

Iaccarino, G., 2008, Quantification of uncertainty in flow simulations using probabilistic methods, Institute for Computational Mathematical Engineering, VKI Lecture Series.

Isaaks, E., 1984, Indicator simulation: Application to the simulation of a high grade uranium mineralization. In *Geostatistics for Natural Resources Characterization*, Par 2. (ed. G.V.e. al.), pp. 1057-1069. D. Reidel Publishing Company

Journel, A., 1992, Geostatistics: Roadblocks and challenges, *in* A. Soares (ed.), Geostatistics-Troia, vol. 1, Kluwer Academic Publications, pp. 213-224.

Journel, A., 2005, Beyond covariance: the advent of multiple-point geostatistics, *in* Geostatistics Banff 2004, Quantiative Geology and Geostatistics, (ed.), Leuangthong, O., and Deutsch, C. V., Springer Netherlands, Dordrecht, Netherlands, pp. 225-233.

Legler, B., Hampson, G. J., Jackson, C. A.-L., Johnson, H. D., Massart, B. Y. G., Sarginson, M., and Ravnas, R., 2014, Facies relationships and stratigraphic architecture of distal, mixed tide- and wave-influenced deltaic deposits: Lower

Sego Sandstone, western Colorado, U.S.A., Journal of Sedimentary Research, 2014, v. 84, pp. 605-625.

Le Loc'h, G., and Galli, A. G., 1994, Improvement in the truncated Gaussian method: combining several Gaussian functions. In *Ecmor 4, 4th European Conference on Mathematics of Oil Recovery*, Roros, Norway.

Mariethoz, G., and Kelly, B. F. J., 2011, Modeling complex geological structures with elementary training images and transform-invariant distances, Water Resources Research, 47.

Mariethoz, G., REnard, P., Carnaton, F., and Jaquet, O., 2008, High-resolution truncated pluriguassian simulations for the characterization of heterogeneous formations, Centre for Hydrogeology.

Matheron, G., 1963, Principles of geostatistics, Economic Geology, v. 58, pp. 1246-1266.

Matheron, G., Beucher, H., Gall, A., Guérillot, D., and Ravenne, C. 1987, Conditional simulation of the geometry of fluvio-deltaic reservoirs. In *62nd Annual Technical Conference and Exhibition of the Society of petroleum Engineers*, pp. 591-599. SPE Paper 16753, Dallas.

McLaurin, B. T., and Steel, R. J., 2000, Fourth-order nonmarine to marine sequences, middle Castlegate Formation, Book Cliffs, Utah, Geology, v. 28, no. 4, pp. 359-362.

Michael, H., Gorelick, S., Sun, T. Li, H, Boucher, A and Caers, J., 2009, Combining geologic-process models and geostatistics for conditional simulation of 3-D subsurface heterogeneity, Water Resources Research, 46.

Montgomery, D. C., and Peck, E. A., 1982, Introduction to linear regression analysis: New York, John Wiley, p. 527.

Narayanan, K., 1999, Applications for response surfaces in reservoir engineering: Unpublished M.S. thesis, University of Texas at Austin, pp. 90.

Painter, C. S., York-Sowecke, C. C., and Carrapa, B., 2013, Sequence stratigraphy of the upper Cretaceous Sego Sandstone member reveals spatio-temporal changes in depositional processes, northwest Colorado, U.S.A., Journal of Sedimentary Research, v. 83, pp. 323-338.

Pejman, T., 2012, Multiple-point geostatistical modeling based on the cross-corelation functions, Computational Geosciences, v. 16, no 3, pp 779-797.

Pickering, K. T., Hiscott, R. N., and Hein, F. J., 1989, Deep Marine Environments, Clastic Sedimentation and Tectonics, pp. xiv-416, London: Unwin Hyman. (book).

Steel, R. J., Plink-Bjorklund, P., and Aschoff, J. L., 2012, Tidal deposits of the Campanian Western Interior Seaway, Wyoming, Utah and Colorado, USA, *in* Davis, R. A. Jr., and Dalrymple, R. W., eds., Principles of Tidal Sedimentology: Dordrecht, Springer, pp. 437-471.

Strebelle, S. B., 2002, Conditional Simulation of Complex Geological Structures Using Multiple-Point Statistics: Mathematical Geology, vol. 34, no. 1, pp. 1-21.

Strebelle, S. B., 2006, Sequential simulation for modeling geological structures from training images, *in* T. C. Coburn, J. M. Yarus, and R. L. Chambers, eds., Stochastic

modeling and geostatistics: Principles, methods, and case studies, volume II: AAPG Computer Applications in Geology 5, pp. 139-149.

Tyler, N., and Finley, R. J., 1991, Architectural controls on the recovery of hydrocarbons from sandstone reservoir, *in* A. D. Miall and N. Tyler, eds., the three dimensional facies architecture of terrigenous clastic sediments and its implications for hydrocarbon discovery and recovery: SEPM Concepts in Sedimentology and Paleontology, v. 3, p. 1-5.

Van Wagoner, J. C., 1991, High-frequency sequence stratigraphy and facies architecture of the Sego Sandstone in the Book Cliffs of western Colorado and eastern Utah; *in* J. C. Van Wagoner, D. Nummedal, C. R. Jones, D. R. Taylor, D. C. Jennette, and G. W. Riley, eds., Sequence stratigraphy applications to the shelf sandstone reservoirs: outcrop to subsurface examples: AAPG field Conference, Tulsa, Oklahoma, pp. 1-22.

White, C. D., and Barton, M. D., 1997, Comparison of the recovery behavior of contrasting units in the Ferron sandstone using outcrop studies and numerical simulation: The University of Texas at Austin, Bureau of Economic Geology, topical report prepared for the Gas Research Institute, GRI-97/0095.

White, C. D., and Barton, M. D., 1999, Translating outcrop data to flow models, with applications to the Ferron Sandstone: Society of Petroleum Engineers Reservoir Evaluation and Engineering, v. 2, no. 4, p. 18.

White, C. D., Willis, B. J., Dutton, S. P., Bhattacharya, J. P., and Narayanan, K., 2004, Sedimentology, statistics, and flow behavior for a tide-influenced deltaic sandstone, Frontier Formation, Wyoming, United States, *in* Integration of outcrop and modern analogs in reservoir modeling: AAPG Memoir 80, pp. 129-152.

Willis, B. J., and White, C. D., 2000, Quantitative outcrop data for flow simulation: Journal of Sedimentary Research, v. 70, pp. 788-802.

Willis, B. J., and Gabel, S., 2001, Sharp-based, tide-dominated deltas of the Sego Sandstone, Book Cliffs, Utah, U.S.A.: Sedimentology, v. 48, pp. 479-506.

Willis, B. J., and Gabel, S., 2003, Formation of deep incisions into tide-dominated river deltas; implications for the stratigraphy of the Sego Sandstone, Book Cliffs, Utah, U.S.A, in Gabel, S.L., ed., Journal of Sedimentary Research, Volume 73: Untied States, Society of Economic Paleontologists and Mineralogists: Tulsa, OK, United States, p. 246-263.

Wood, L.J., and Willis, B.J., 1999, Sequence stratigraphy and reservoir architecture of tide-influenced shoreline systems in the Late Cretaceous Sego Sandstone: Bureau of Economic Geology Field Trip Guide, Austin, Texas.

Wood, L.J., 2004, Predicting tidal sand reservoir architecture using data from modern and ancient depositional systems, AAPG Memoir, Volume 80: United States, American Association of Petroleum Geologists: Tulsa, OK, United States, p. 45-66.

Wood, L.J., Flaig, P. P., and Van der Kolk, D. A., 2014, Wave, tide, and river-dominated systems of the Cretaceous Western Interior Seaway: The Kenilworth and Grassy Members of the Blackhawk, the Sego, and the Loyd Formations, eastern Utah and

northwestern Colorado, Bureau of Economic Geology Field Trip Guide, Austin, Texas.

Yoshida, S., Miall, A. D., and Willis, A., 1996, Sequence stratigraphy and marine to non-marine facies architecture of foreland basin strata, Book Cliffs, Utah, U.S.A.: Reply: American Association of Petroleum Geologists, Bulletin, v. 82, p. 1596-1606.